POLITECNICO DI TORINO

Department of Mechanical and Aerospace Engineering
Master's Degree Course in Aerospace Engineering

Master's Degree Thesis

Forced response and wear volume consumption of an LPT tip shrouded blade

Supervisors
Prof. Giuseppe Battiato
Prof. Daniele Botto
Ing. Antonio Giuseppe D'Ettole

Candidate
Daniele Bertrando 290606

Academic Year 2022/2023

Per aspera sic itur ad astra

Acknowledgment

Un grazie speciale alla mia famiglia, alla mia ragazza Rebecca, ai miei vecchi amici delle scuole superiori e a tutti gli amici che ho conosciuto durante il percorso universitario al Politecnico.

Abstract

In the last years, the aeronautical industry has had a continuous growth and expansion and the aircraft manufacturers have focused their efforts on improving efficiency and performance of existing engines. Most of these improvements come from recently developed analyses techniques applied to the main engine's components. One of them is the Low-Pressure Turbine (LPT) which has a fundamental part on the overall efficiency of an aircraft engine. The design process of an LPT involves several disciplines such as Aeromechanics, Rotordynamics, Aeroelasticity. For these reasons, this thesis, carried out in collaboration with GE Avio Aero, is focused on the study of forced response analyses and wear behavior of a tip shrouded blade of a Low-Pressure Turbine. In particular, the main topic is the study of the impact of changing the interlocking angle on the dynamic behavior of the blades. In fact, an excessive wear at the interlocking interface can change the dynamic behavior, causing HCF failures due to the occurrence of unavoidable resonance. The study is conducted on two different blade configurations, i.e. Baseline and Redesign models. The analyses are performed using several commercial software such as Hypermesh, Ansys APDL and Matlab. Furthermore, the numerical tools Policontact and Poliwear are used for forced response analyses and for the evaluation of the wear behavior, respectively. The study is carried out for an industrial blade, therefore only the qualitative results will be reported.

Contents

List of Figures

Chapter 1

Introduction

1.1 E-TDCs: European Technology Development Clusters

This thesis work is referred to the E-TDCs, European Technology Development Clusters, launched in May 2020, that is a network operating into the Research and Innovation Field, with a unique collaborative model in Europe, whose members work together under one single framework agreement which defines financial provisions, IP rules, dissemination, and publications.

The E-TDCs include up today 33 parties: 22 Research Institutions, 3 SMEs and 8 GE Affiliates, see Fig. 1. The Academia, Research Centers and SMEs involved have proven technical and scientific skills, as well as unique experimental assets and expertise in the collaborative Research and Innovation environment. The E-TDCs count 10 different Clusters, consisting of Research Institutions and GE Aviation teams, each of them focused on dedicated disciplines or products of GE Aviation interest, set up taking into consideration the complementarity of knowledge and operating on the basis of an Innovation Plan with the following responsibilities:

- to execute and monitor the Innovation Plan and monitor the international scientific scenario.
- to leverage the complementary knowledge and capability of teams.

- to propose, where necessary, extension of the collaboration to other research teams.
- to promote, where necessary, integration with SMEs.
- to evaluate financing opportunities through participation external funded projects.
- to manage publications and events to disseminate the results obtained.
- to identify, train and involve new talent, including through degree theses, PhD, etc...
- to develop skills and highly specialized human resources.

Figure 1: E-TDCs Network and Clusters

The network extension and the Clusters progress, results, and ongoing plans are overseen trough a well-established Governance structure, see Fig. 2, which defines Operating Rhythm and key actors. Just on November 25th it has been held the 2021 edition of the E-TDCs Annual Event: LKD.

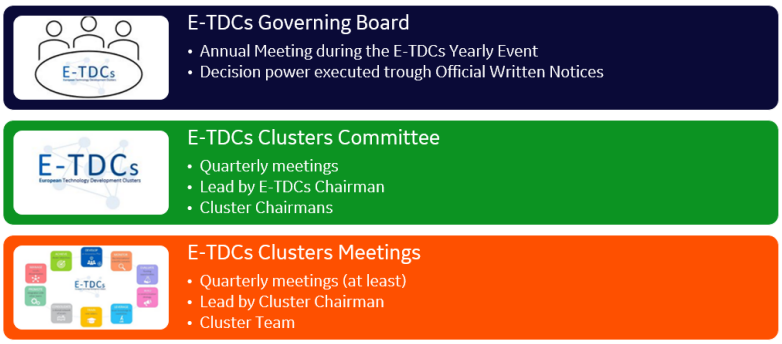

Figure 2: E-TDCs Governance

This work of thesis has been done in the Aeromechanics Cluster focused on research activities related to HCF (High Cycle Fatigue) problems due to forced response and Flutter. This discipline has become of great interest for the designers, as it allows to predict the safety margins of critical components so that high-performance engines can operate safely.

Chapter 2

Aircraft Engine

The main function of an aircraft engine is to provide thrust for the sustenance of the plane. During history propulsion, many engineers created different solutions depending on the complexity and the category of the aircraft. All the aircraft engines based their functioning on the Newton's Third Law (Principle of action and reaction):

"For each action there is an equal and opposite reaction"

This principle is related to the conservation of momentum. The flow deflection due to the shape of the blades (airfoil) caused a pressure distribution that generate a force (called Lift) and accelerate the flow.

2.1 Jet Propulsion

Historically, the first jet propulsion engine was patented in 1913 by René Lorin, a French engineer who designed it, but he never manufactured or used it. The main reasons concerned the lack of proper technologies because suitable heat resisting materials were not developed yet and the engine would have been too inefficient at the low speeds. At those days, time was not yet ripe, and we had to wait until 1930 to see the first gas turbine used on a propulsive jet. It was developed by Sir Frank Whittle, an English engineer, inventor, and RAF air officer. He formulated the fundamental concepts that led to the creation of the turbojet engine, but the

first flight was completed only 11 years later. Today it can be said that his work set the basis for the modern gas turbine engine.

The aircraft engines are divided in many classes, but in this thesis, we only deal with airbreathing engines. Their function is taking the air from the outside, accelerating, and expelling it at high speed. The thrust is proportional to airflow rate, so the objective during the design process is to maximize the airflow rate per unit size of engine (i.e., maximizing the entering air speed and the fraction of the inlet area devoted to airflow). Inside the engine, the airflow is energized by compressing and heating it. At high flight speeds, jet propulsion is more efficient than propeller propulsion, because the latter become noisy and its performance decreases at Mach number 0.5 or 0.6.

The purpose of a jet engine is the production of thrust and the resultant forces acting on the engine is given by the general thrust equation:

$$F = \dot{m}_e v_e - \dot{m}_0 v_0 + (p_e - p_0)A_e$$

In this equation we can highlight the mass rate $\dot{m}$, the air flow velocity v and the pressure p. The subscript 0 refers to the entering quantities whereas the subscript e refers to the exit of the engine. According to this equation, the same thrust can be obtained either by giving a large velocity to a small mass of air or vice-versa (a small velocity to a large mass of air). For a higher propulsive efficiency, it is preferred the second option and that is the reason why the actual trend in propulsion design is to create larger front section of the engine.

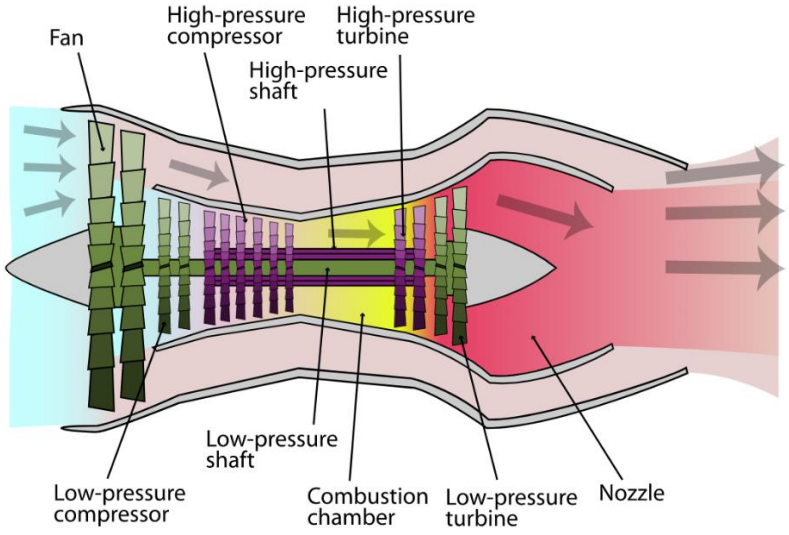

Figure 3: Basic components of an aircraft engine [18]

The architecture of an aircraft engine can be very complex, so it will be useful to study a cross-section and highlight the main components that made up a turbofan engine.

1) ***Air Intake*** → It is the interface between external environment and the engine's first component. Intake is an opening structure where the fluid is admitted due to a pressure difference between the outside and the inside. This pressure differential is generated by the compressor downstream the intake and the flow rate will depend not only on this difference, but also on fluid properties and intake geometry. The main goals of an intake are:

    - Provide the thruster with a given flow rate at a given Mach
    - Minimize total pressure loss and flow distortions to achieve a uniform flow upstream of the compressor
    - Minimize aerodynamic drag, weight, and length

2) ***Fan and Low-Pressure Compressor (LPC)*** → Fan is a particular low-pressure compressor that compresses air into a by-pass duct and divided it into hot air flow and cold air flow. In that way, only one flow goes through all the engine's components while the cold air flow goes directly to the exhaust system. So, Fan contributes to the engine's thrust by accelerating the cold air flow. LPC consists of one or two stages and, in a two-spool engine configuration, LPC and Fan are connected to a low-pressure shaft, which is driven by a low-pressure turbine. The LPC's function is to perform an initial compression of the air flow. Each compressor stage is formed by a stator following the rotor.

3) ***High pressure compressor (HPC)*** → HPC has several stages (usually 10 or more), and it is connected to a high-pressure shaft, which is driven by a high-pressure turbine. Typical compression rates are about 30 or higher, so the flow can reach over than 900 K temperature.

4) ***Combustion chamber (combustor)*** → It is the component where combustion takes place. The combustor is fed high-pressure air by the compressor and then heats it at constant pressure. When the fuel/air mix burns, it heats and quickly expands. So, the turbine stages take a smooth stream of heated gas at all conditions required. Inside the combustion

chamber, the temperatures are limited by the material of the turbine blades and nozzles, and they are usually in the range of 1200 K to 2000 K. There are many types of combustors such as can type, cannular type and annular type.

5) ***High pressure turbine (HPT)*** → The main function of a turbine is to provide the power to drive the compressor. Turbines have less stages than compressors, typically 2 or 3, each one formed by a rotor following the stator. The stages are designed to provide an expansion of the flow and the pressure drop can be much greater than the pressure increase across a corresponding compressor stage. The flow comes from the combustion chamber, so the choice of material is essential, because the HPT interfaces with very high temperature.

6) ***Low pressure turbine (LPT)*** → LPT is connected to the low-pressure shaft, so its function is to drive the LPC and Fan. Usually, the number of stages is 1 or 2 and they are designed for low values of pressure ratio. The partition in LPT and HPT reduces the mass flow rate of air to elaborate, maintaining the same thrust.

7) ***Exhaust system (Nozzle)*** → Nozzle is the device designed to control the direction of the fluid flow and discharge the turbine exhaust gases to atmosphere, in order to provide thrust. Its shape has an important influence on the performance of the engine, so the areas must design accurately.

So, the gas turbine is essentially a heat engine that uses air as a working fluid. The engine working cycle is the *Brayton Cycle*, which is composed by four phases:

a) 1 – 2 → compression of atmospheric air (isentropic process), where the air is drawn into the compressor stages, which pressurized it. To determine the efficiency of the engine, it is usually used the compression ratio, defined as

$$\beta = \frac{p_2}{p_1}$$

The efficiency of the transformation is directly proportional with this design parameter. In modern engine architecture the compressor is divided into two major units (i.e., LPC and HPC).

b) 2 – 3 → combustion of compressed air (isobaric process), where the fuel (usually Kerosene) is burned, and a combustion chamber heats the compressed air. This phase takes place at constant pressure in the idealized Brayton cycle, but in real cycle the pressure losses are not negligible. The efficiency of the combustion depends on the homogeneity of the mixture, so this is the reason why, in the modern engine architecture, an air-fuel mixture configuration takes place upstream the combustion chamber. The choice of thermo-resistant materials is essential to allow engine components handling higher temperatures (i.e., overall higher efficiency).

c) 3 – 4 → expansion (isentropic process), where the air is expanded through one or more turbines and the work extracted by them is used to drive the compressor. Each turbine stage is composed by a vane (steady component row) and a set of blades (rotor component row). Due to the airfoil shape, the motion produces a pressure difference between Pressure Side and Suction Side of the blades.

d) 4 – 1 → exhaust (isobaric process), with heat rejection in the atmosphere through the nozzle, which ensures an increase of speed that will translate into an increase of the reaction force act on the aircraft

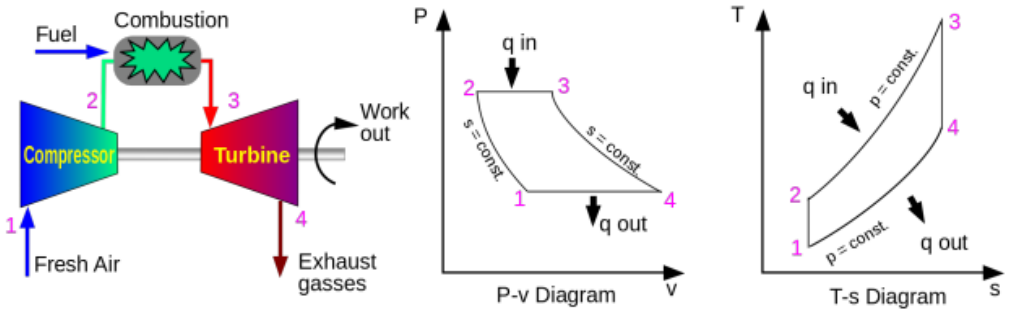

Figure 4: Ideal Brayton-Joule cycle [20]

The efficiency of the ideal Brayton cycle is given by this equation,

$$\eta = 1 - \frac{T_1}{T_2} = 1 - \left(\frac{p_1}{p_2}\right)^{\frac{\gamma-1}{\gamma}}$$

where γ is the heat capacity ratio. The area under the T-s diagram is proportional to the work and thrust generated by the engine.

It is conventionally assumed that the exhaust gases are reused in the intake, but the cycle is usually run as an open system (so the gases are exhausted in the atmosphere).

For increasing the power output of a Brayton engine, a solution is the reheat, using an afterburner where the reheated air is expanded through a thrust nozzle rather than a turbine.

2.2 Turbojet

Turbojet engines are used instead of turboshafts for flying at higher Mach number. They have lower efficiency at low speeds than turboshafts, and they consist of a gas turbine with a propelling nozzle. These engines have the task of producing thrust, according to the principle of action and reaction and they can be equipped with an afterburner, which is a combustion chamber added to reheat the turbine exhaust gases. Afterburners are used exclusively at supersonic speed, especially in military aircrafts.

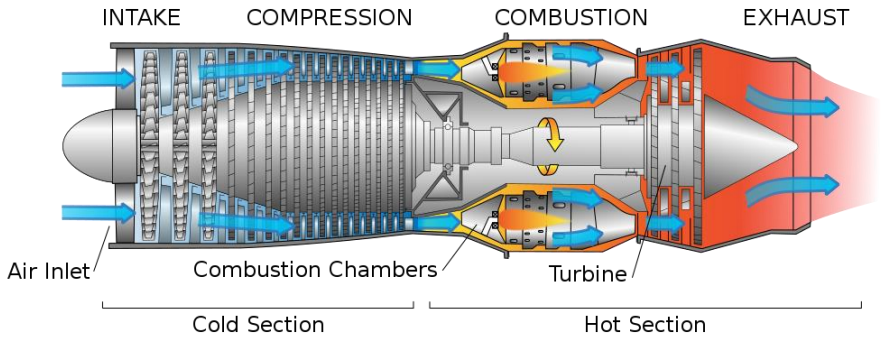

Figure 5: Turbojet engine [16]

The main components of a turbojet are inlet, compressor, combustor, turbine, and propelling nozzle. There are many configurations such as a twin-spool in which

the compression and the expansion are split among two stages of compressor and turbine, to maintain a high efficiency in all compressor stages. So, in this configuration, there is a LPC driven by a LPT and a HPC driven by an HPT.

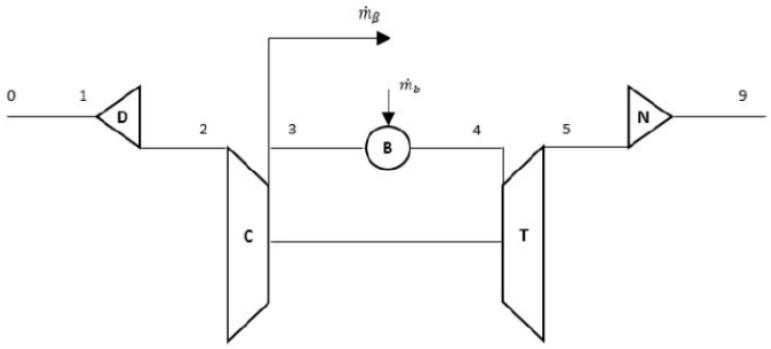

Figure 6: Turbojet engine sketch

2.3 Turboshaft

The main function of a turboshaft is to produce mechanical work (power) instead thrust, and its power is used by one or more propellers or a rotor through transmission shafts. This category of engines extracts work from the fluid in the turbine and uses it to move the compressor and the propellers. Turboshafts are generally used on helicopters and in all applications that require a sustained high-power output.

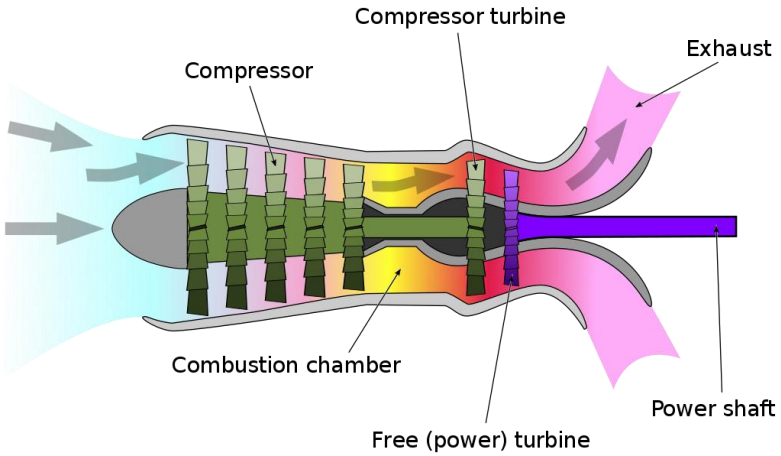

Figure 7: Turboshaft engine [17]

A turboshaft engine is made up by:

- A gas generator, which includes compressor, combustion chamber with ignitors and fuel nozzles and the turbine stages. His function is to extract energy during the expansion of hot gases and drive it to the power section.
- A power section, that consists of additional stages of turbine, a gear reduction system, and the shaft output.

Depending on the engine, the accessories may be driven by the gas generator or by the power section.

An important configuration of turbofan is the free-turbine turboshaft, where gas generator and power section are mechanically separate and the power is extracted from the exhaust stream of gas turbine by an independent turbine, downstream of the gas turbine. The main advantage of the free-turbine turboshaft is that the gas generator and the power section can operate at different speeds appropriate for the conditions.

An example of application of a turbofan engine is the Sikorsky CH-53E Super Stallion, an US cargo helicopter which uses three General Electric T64 at 4,380 hp each.

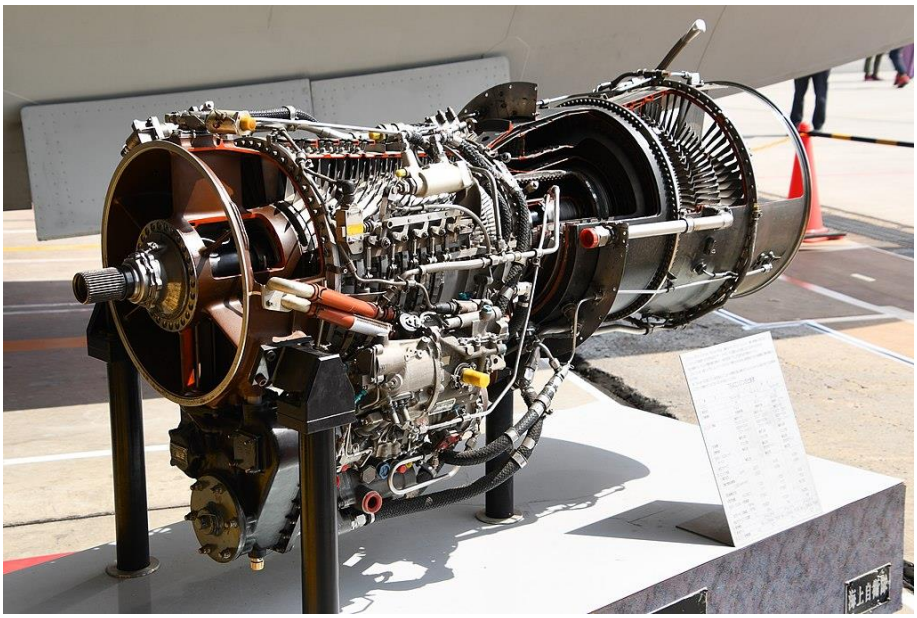

Figure 8: General Electric T64 [22]

2.4 Turbofan

Turbofan's architecture is an evolution of turbojet engine, and it was invented to optimize the fuel consumption of the turbojet. The main innovation is that there isn't a single core flow, but the fan separates the flow into a cold and a warm flow that follow two different paths inside the engine. The warm flow passes through all the stages of the engine while the cold flow:

- For low-bypass turbofan, passes through fan and nozzle.
- For high-bypass turbofan, passes through only the fan.

The bypass ratio (BPR) is the ratio between the mass flow rate of the bypass stream to the mass flow rate entering the core. Engines with more jet thrust relative to fan thrust are known as low-bypass turbofans and they are typically used on modern fighter. Instead, engines with more fan thrust are called high-bypass turbofans and they are in commercial aviation.

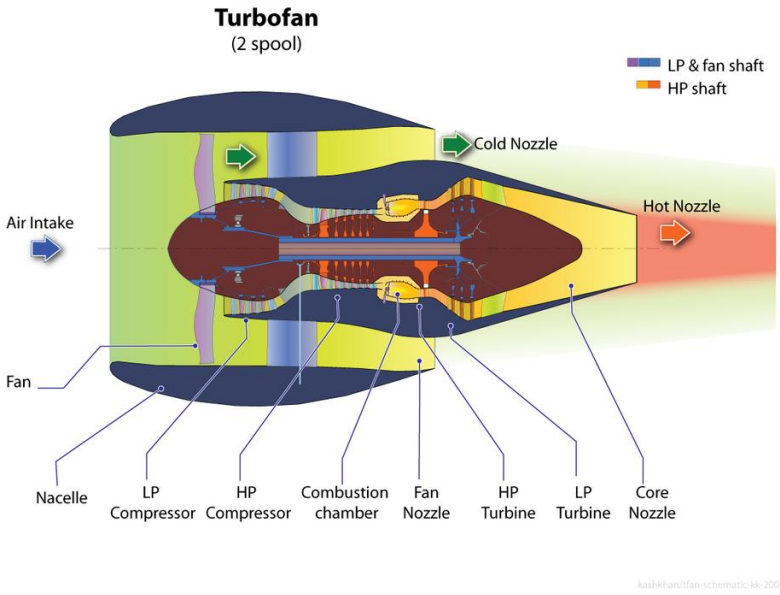

Figure 9: Turbofan engine [18]

Turbofans are the most efficient engines in the range of speeds from 500 to 1000 km/h, which is the speed of most commercial aircraft. The propulsive efficiency can be defined as:

$$\eta_f = \frac{2}{1 + \frac{V_j}{V_a}}$$

In this equation it is possible to highlight the thrust equivalent jet velocity V_j and the aircraft velocity V_a. The extraction and transfer to a bypass system of shaft power introduces extra losses. The additional losses in a turbofan are due to its great number of compressor stages, fan, and bypass duct.

An example of a known turbofan engine is the GE90, used on Boeing 777, which is the most powerful aircraft engine with a maximum thrust of 510 kN.

Figure 10: GE90 [21]

2.5 Turboprop

Turboprop engine is very similar to the turbofan, but the power extracted from hot flow is not given to a fan, but it drives an aircraft propeller. Turbine shaft and propeller are connected by an adaptor and the engine can have one or more shafts.

The main components of a turboprop are intake, reduction gearbox, compressor, combustor, turbine, and a propelling nozzle. The engine's exhaust gases do not provide thrust, because all the power is used to drive the propeller. The shaft power is obtained by extracting additional power from turbine expansion, so the residual energy in the exhaust gases is too low to generate a consistent thrust (that is only about 10% of the total thrust).

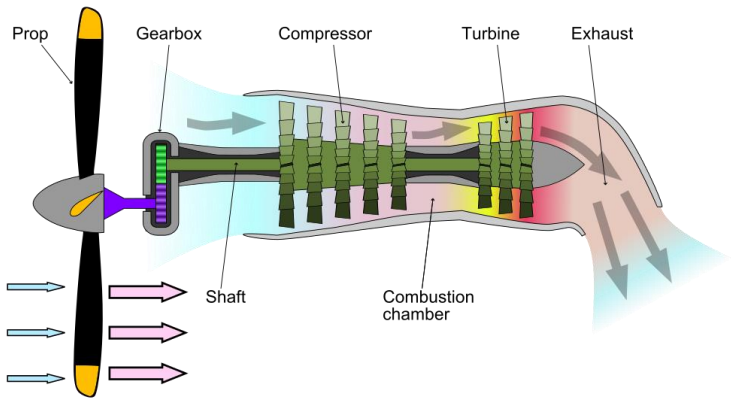

Figure 11: Turboprop engine [19]

Propeller and turbine are coupled through a reduction gear, which function is to convert the high RPM and low torque output to low RPM and high torque. Propeller is normally a constant-speed propeller type to maintain its efficiency across a wide range of airspeeds.

Turboprops have a large diameter that lets it accelerate a high flow rate and this permits to obtain an amount of thrust. For this reason, it is more efficient at low speeds, so it works well until the flight speed is less than 0.6 – 0.7 Mach. Comparing to the turbofan, turboprop has less specific consumption, because the propeller is able to process a great flow rate with high bypass ratio (which can be in a range of 50-100).

Chapter 3

Rotordynamics

Rotordynamics is a branch of systems dynamics concerned with at least one mechanical structure, usually defined as ***rotor***, which rotates with significant angular momentum around an axis. Rotor is bound to the fixed part of the machine by bearings, which allow motion rotation minimizing the friction between the fixed part and the rotating part.

3.1 Dynamics of the bladed discs

In turbomachinery, rotors are elastic elements, and they are not infinitely rigid, so if the amplitude of vibration at critical speeds is too high, then catastrophic failure occurs.

An example are bladed discs of turbine and compressor typically used on aircraft engines. These components are made up by N identical sectors that form a complete 360° model. The task of the dynamic analysis is to avoid resonance conditions into the machine's operative range or to control the amplitude of vibration by introducing additional damping. The first step of analysis is the modal analysis, which identify the natural frequencies and the own modes. Then, it will be necessary to verify the presence of resonances and calculate the amplitude of the response.

This kind of analysis can be performed using the so-called ***cyclic symmetry***.

3.2 Cyclic symmetry

Bladed discs of turbine and compressor are rotational periodicity or cyclic symmetry structures, so they can be described by a finite number of identical substructures or sectors forming a closed geometry. The main advantage of these structures is that the geometry for any radial and axial position at a certain angle θ is identical to the geometry at the angular position $\theta + n\alpha_n$.

The sector angle can be defined as:

$$\alpha_n = \frac{2\pi}{N}$$

Where N represents the number of disc's sectors and $n = 1, \dots, N$ is the current sector which is considered.

For the evaluation of natural frequencies and mode shapes, the procedure performed is the *Finite Element* (FE) analysis, also known as meshing. It consists of switching from a continuous structure into a discrete mathematical model, in which the structure is discretized in a certain number of elements.

The simplest model to use is the model at 2 degrees of freedom each sector. In fact, considering the adjacent sectors, it is possible to build the complete 360° model and coupling the adjacent sectors together.

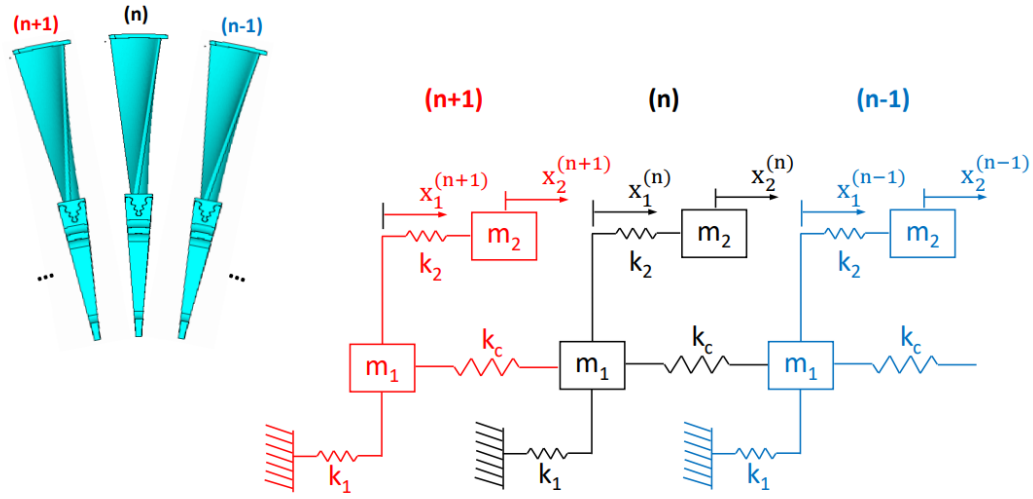

Figure 12: Example of a cyclic symmetry model [15]

For the generic sectors n, the equilibrium equations are:

1) $m_1\ddot{x}_1^n + k_1 x_1^n + k_2(x_1^n - x_2^n) + k_c(x_1^n - x_1^{n+1}) + k_c(x_1^n - x_1^{n-1}) = 0$
2) $m_2\ddot{x}_2^n + k_2(x_2^n - x_1^n) = 0$

They can also be written in matrix form:

$$\begin{bmatrix} m_1 & 0 \\ 0 & m_2 \end{bmatrix} \begin{Bmatrix} \ddot{x}_1^n \\ \ddot{x}_2^n \end{Bmatrix} + \begin{bmatrix} k_1 + k_2 + 2k_c & -k_2 \\ -k_2 & k_2 \end{bmatrix} \begin{Bmatrix} x_1^n \\ x_2^n \end{Bmatrix} + \begin{bmatrix} -k_c & 0 \\ 0 & 0 \end{bmatrix} \begin{Bmatrix} x_1^{n+1} \\ x_2^{n+1} \end{Bmatrix} + \begin{bmatrix} -k_c & 0 \\ 0 & 0 \end{bmatrix} \begin{Bmatrix} x_1^{n-1} \\ x_2^{n-1} \end{Bmatrix}$$

These equations are valid for all sectors.

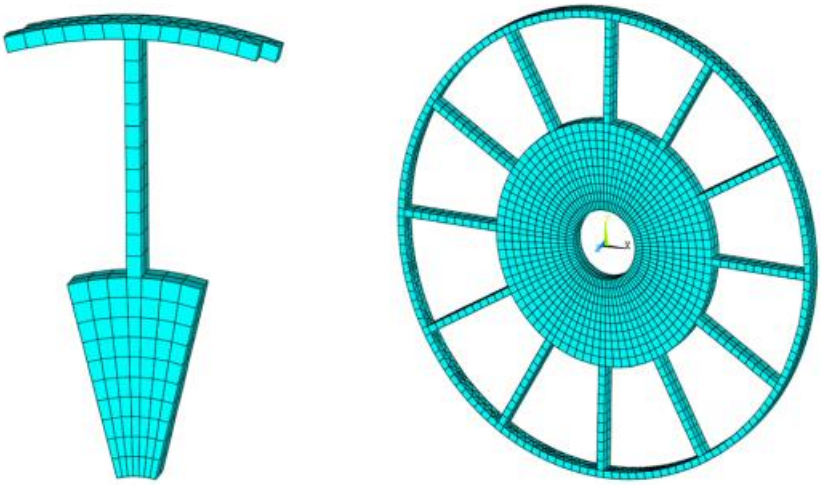

Figure 13: FE model of a bladed disk and the single-sector model [7]

In a different way, the bladed disc can be studied as a *Multi Degrees of Freedom* system, with linear and conservative equation of motion that can be written in the following general matrix form:

$$[M]\{\ddot{x}(t)\} + [K]\{x(t)\} = F(t)$$

Where:

- $x(t)$ is the vector of degrees of freedom
- $\ddot{x}(t)$ is the acceleration vector
- M is the mass matrix

- K is the stiffness matrix
- $F(t)$ is the vector of external forces

For N total number of nodes resulting from the structure discretization, the size of matrices and vectors are the following:

$$M \in \mathbb{R}^{3N\times 3N} \qquad K \in \mathbb{R}^{3N\times 3N} \qquad x(t) \in \mathbb{R}^{3N\times 1} \qquad f(t) \in \mathbb{R}^{3N\times 1}$$

For cyclic symmetry structures, the equation of motion will be written in a cylindrical coordinate system with the z-axis coinciding the structure's revolution axis. Also, it is useful to rearrange vectors and matrices so that n_s DOF of the 1^{st} sector is followed by n_s DOF of the 2^{nd} sector and so on.

$$M = \begin{bmatrix} M_0 & M_1 & M_2 & \dots & M_2 & M_1 \\ M_1 & M_0 & M_1 & \dots & M_3 & M_2 \\ M_2 & M_1 & M_0 & \dots & M_4 & M_3 \\ \vdots & \vdots & \vdots & \ddots & \vdots & \vdots \\ M_2 & M_3 & M_4 & \dots & M_0 & M_1 \\ M_1 & M_2 & M_3 & \dots & M_1 & M_0 \end{bmatrix} \qquad x = \begin{Bmatrix} x_1 \\ x_2 \\ x_3 \\ \vdots \\ x_{N-1} \\ x_N \end{Bmatrix} \qquad f = \begin{Bmatrix} f_1 \\ f_2 \\ f_3 \\ \vdots \\ f_{N-1} \\ f_N \end{Bmatrix}$$

$$K = \begin{bmatrix} K_0 & K_1 & K_2 & \dots & K_2 & K_1 \\ K_1 & K_0 & K_1 & \dots & K_3 & K_2 \\ K_2 & K_1 & K_0 & \dots & K_4 & K_3 \\ \vdots & \vdots & \vdots & \ddots & \vdots & \vdots \\ K_2 & K_3 & K_4 & \dots & K_0 & K_1 \\ K_1 & K_2 & K_3 & \dots & K_1 & K_0 \end{bmatrix}$$

Within the matrices M and K, they can be isolated the submatrices M_h and K_h, which are ***block circulant symmetric structure*** whose dimensions coincide with the number of each sector's DOFs. The parameter h is a function of N:

- If N is even, $h = 0, \dots, \frac{N}{2}$
- If N is odd $h = 0, \dots, \frac{N-1}{2}$

So, from the FE model, the mass and stiffness matrices are obtained and then, mode shapes and natural frequencies can be found by solving the following eigenproblem:

$$(K - \omega_i^2 M)u_i = 0 \qquad i = 1, \dots N \cdot n_s$$

The i^{th} eigenvector u_i can be written as:

$$u_i = \left[(u_{1_i})^T \quad (u_{2_i})^T \quad \dots \quad (u_{N_i})^T \right]^T$$

The modal displacements of the n^{th} substructure are containing in the vector u_{n_i}. For the cyclic symmetry structures, most vibration modes occur in orthogonal pairs and the rotation of the same mode through an integer multiple of the sector angle α_n does not change the corresponding frequency of vibration.

So, for this category of structures, there are three classes of mode shapes:

A. $u_{n_i} = u_{(n+1)_i} \quad \forall n$

In this case, mode shape of a sector is the same of the adjacent sectors and vibrates in-phase with them. The consequence is that the mode shape does not change rotating it through any arbitrary number of sectors. It is called "standing wave" mode shape and it is described by a single eigenvalue and eigenvector.

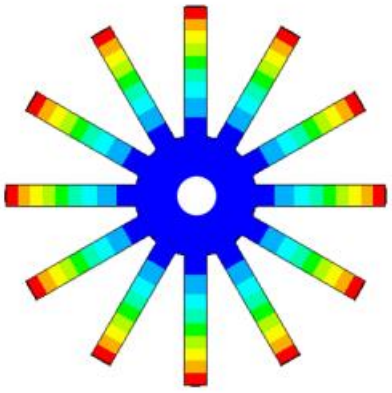

Figure 14: Example of blades vibrating in phase with each other [3]

B. $u_{n_i} = -u_{(n+1)_i} \quad \forall n$

As in the previous case, each sector has the same mode shape as the adjacent sectors, but it vibrates in anti-phase with them. If the rotation of the mode shape is an even number of sections, the mode shape does not change. But, if the rotation is an odd number of sections, the mode shape has inverted sign meaning that it changes of phase of π.

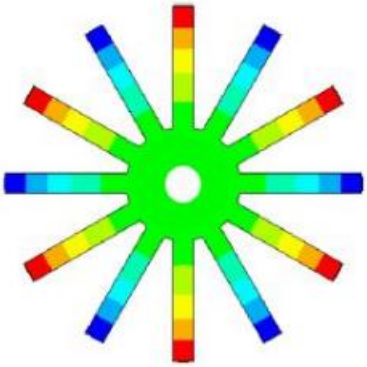

Figure 15: Example of blades vibrating in anti-phase with each other [3]

C. $u_{n_i} \neq u_{(n+1)_i} \quad u_{n_i} \neq -u_{(n+1)_i} \quad \forall n$

These are all other possible mode shapes, and they occur in orthogonal pairs of standing waves with the same eigenvalue, so their combination results in a rotating mode shape. The periodicity of mode shape can be expressed through the number of nodal diameters (in cyclic symmetry structures a nodal diameter is defined as the line of aligned points crossing the center of rotation consisted of null nodal displacements)

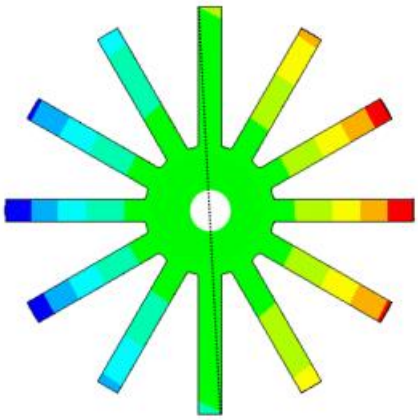

Figure 16: Example of blades with a rotating mode shape [3]

If all sectors are identical, all the mode shapes have the same eigenvalue for each sector angle. So, it is possible to identify a basis that represent the

set of all the possible eigenvectors obtained by sequential shifts of u_i each one by the sector angle:

$$U_i = [u_i \quad \bar{u}_i]$$

The eigenvector $\bar{u}_i$ has the same eigenvalue ω_i^2 of u_i and it is defined as:

$$u_i^T \bar{u}_i = 0$$

As a linear combination of u_i and $\bar{u}_i$, the eigenvector u_i' can be expressed as:

$$u_i' = a u_i + b \bar{u}_i \qquad a, b \in \mathbb{R}$$

It can be demonstrated that $a = \cos(\varphi)$ and $b = -\sin(\varphi)$, where φ_h is defined as the *Inter Blade Phase Angle* (IBPA), which is the ratio between the number of nodal diameters and the number of blades.

$$\varphi = \pm \frac{2\pi h}{N}$$

The parameter h is called harmonic index and represents the number of nodal diameters of a mode shape. Using IBPA, the eigenvectors can be related each other with a rotation of this angle:

$$u_{n_i} = u_{n-1_i} e^{i\varphi}$$

The angle $\varphi = 0$ $(h = 0)$ corresponds to the mode (A), which modal shape is identical for all sectors.
The angle $\varphi = \pi$ $(h = \frac{N}{2})$ correspond to the mode (B), which modal shapes have inverted sign from one sector to the next. So, this mode exists only if the number of sectors N is an even number.
It remains to study the admissible values of IBPA for complex modes of type (C). Considering the index $0 < h < N/2$ and $\frac{N}{2} < h < N - 1$, these modes have a phase displacement between adjacent sectors:

$$u_{n_i} = u_{n-1_i} e^{ih\frac{2\pi}{N}}$$

Due to the periodicity of the function e^{ix}, it is possible to write:

$$e^{ih\frac{2\pi}{N}} = e^{i\left(h\frac{2\pi}{N}-2\pi\right)} = e^{i(h-N)\frac{2\pi}{N}}$$

So, the phase displacement at the index $h = N - 1$ is the same at $h = -1$ and the phase displacement at $h = N - 2$ is the same at $h = -2$. Also, every phase displacement due to a harmonic index $h > N - 1$ is identical to the phase displacement due to a harmonic index $0 < h < N - 1$.

$$e^{ih\frac{2\pi}{N}} = e^{i\left(h\frac{2\pi}{N}-2k\pi\right)} = e^{i(h-kN)\frac{2\pi}{N}}$$

So, the admissible values of IBPA (i.e., the admissible values of harmonic index) can be reassumed in:

$$0 \leq h \leq \tilde{h} \qquad \tilde{h} = \begin{cases} \dfrac{N}{2} \; if \; N \; is \; even \\ \dfrac{N-1}{2} \; if \; N \; is \; odd \end{cases}$$

In conclusion, once the number of nodal diameters is given, the IBPA between sectors is known and bounded by the type of mode.

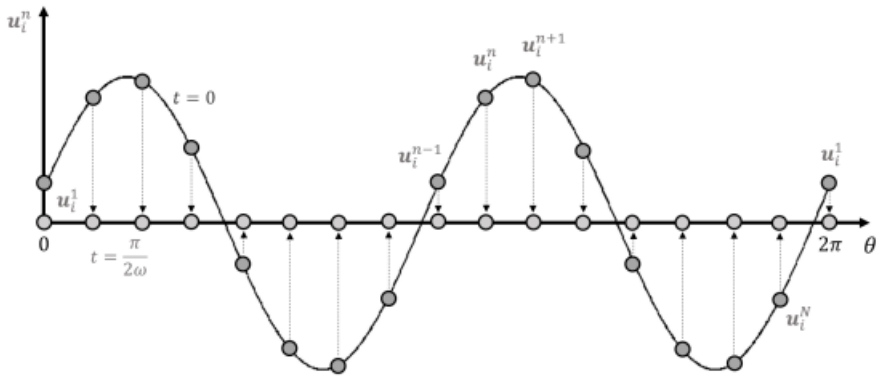

Figure 17: Schematic representation of a standing mode shape for a cyclic symmetry structure [3]

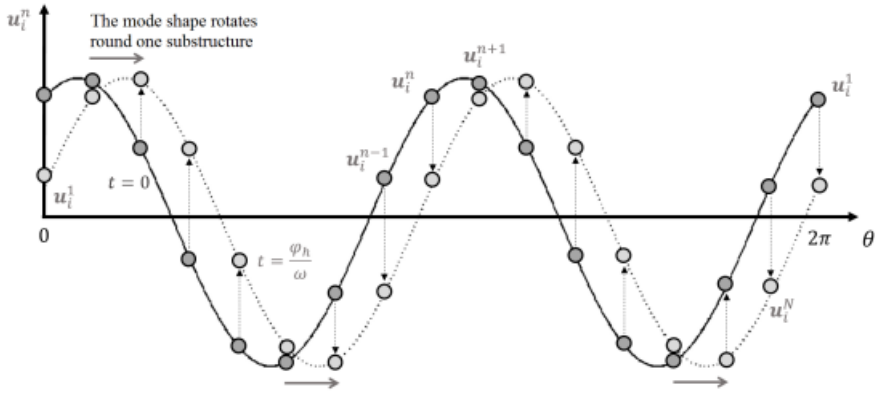

Figure 18: Schematic representation of a rotating mode shape for a cyclic symmetry structure [3]

3.3 Modal analysis in cyclic symmetry

In the previous chapter, it is founded a relation which allows to obtain natural frequencies and mode shapes of cyclic symmetry structures:

$$u_n = u_{n-1} e^{ih\frac{2\pi}{N}}$$

From the motion equation of the fundamental sector, it is possible to obtain a similar expression for the displacements:

$$x_n^1 = x_{n-1}^1 e^{ih\frac{2\pi}{N}} \qquad x_{n+1}^1 = x_n^1 e^{ih\frac{2\pi}{N}}$$

As the harmonic index changes, the motion equations can be written as:

$$(-\omega^2[m_{sc}^h] + [k_{sc}^h])\{x_n\} = 0$$

They can be used for the computation of natural frequencies and mode shapes of the system, without resolving all system. Using the cyclic symmetry propriety, mode shapes of the other sectors can be calculated starting from the adjacent sectors. Proceeding in this way, it will be easy to obtain all mode shapes of the system. The previous equations are referred to a 2 DOFs system, but they can be extended to a finite element model, using the Mead's approach.

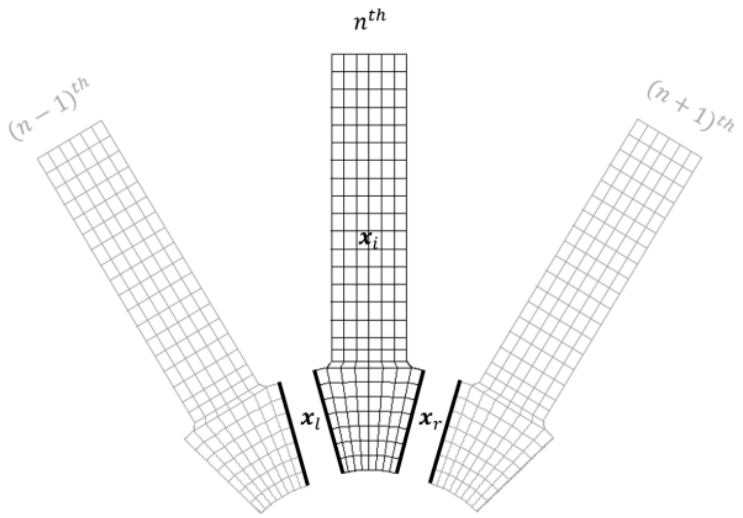

Figure 19: Partition of the fundamental sector [3]

Mead's approach starts with defining a new vector that contains the sector DOFs:

$$x_s = \begin{Bmatrix} x_r \\ x_i \\ x_l \end{Bmatrix}$$

where:

- x_l represents the DOFs at the left interface of the fundamental sector
- x_i represents the internal DOFs of the fundamental sector
- x_r represents the DOFs at the right interface of the fundamental sector

The connection between previous and next sectors is given by x_l and x_r. The left interface of n sector coincides with the right interface of $n+1$ sector.

$$x_s = \begin{Bmatrix} x_r \\ x_i \\ x_r e^{i\varphi h} \end{Bmatrix}$$

Using cyclic symmetry conditions, it is possible to build a transformation matrix $[T]$:

$$x_s = \begin{Bmatrix} x_r \\ x_i \\ x_r e^{i\varphi} \end{Bmatrix} = \begin{bmatrix} I_r & 0 \\ 0 & I_i \\ I_r e^{i\varphi} & 0 \end{bmatrix} \begin{Bmatrix} x_r \\ x_i \end{Bmatrix} = [T]\{x_{sc}\}$$

The new of motion equations obtained by replacing the transformation matrix is:

$$[T]^T(-\omega^2[m] + [k])[T]\{x_{sc}\} = 0$$

Introducing the new matrices $m_{sc} = [T]^T[m][T]$ and $k_{sc} = [T]^T[k][T]$, the system will be:

$$(-\omega^2[m_{sc}^h] + [k_{sc}^h])\{x_{sc}^h\} = 0$$

3.4 Forced Response

The results from modal analysis are useful to obtain natural frequencies and mode shapes of the system. However, if one or more natural frequencies falls into or near the frequency range of forcing, the calculation of the forced response is necessary. For bladed discs, when the rotating blades pass through flow defects created by the interactions of upstream and downstream blade rows, large unsteady aerodynamic forces take place, and they can cause a range of vibration levels. This phenomenon is called forced response.

3.4.1. Loads classification

Firstly, it is necessary to make a classification of the main loads affecting a low-pressure turbine. They can be divided in:

- Quasi-static loads, related to dynamic phenomena with very slow time variation, such as constant or limited time variation forces. Generally, for hypothesis, they are assumed as static loads for the purposes of analysis
- Dynamic loads, such as time-depending forces whose amplitude changes significantly over time. They are usually harmonic forces that produce vibration.

The main static loads that interest a low-pressure turbine are:

- Centrifugal loads, due to the high rotation speeds that make inertial loads on the rotors not negligible. Using r for the generic radial position on the blade and R for the maximum radius, the centrifugal force can be expressed as:

$$F_c = \int_r^R dF_c = \rho\omega^2 \int_r^R rdV = \rho\omega^2 \int_r^R rA(r)dr$$

According to this equation, the most stressed sections are those with a low radius.

- Thermal loads, due to the exposure to exhaust gases with very high temperature. It is responsible of the thermal expansion of the structures, described by the following relation:

$$\epsilon_T = \alpha\Delta T$$

where ϵ_T is the deformation and α is the thermal expansion coefficient. If the component is bounded or the coefficient α is not a constant value, thermal expansion may produce some stresses on the structure. The most dangerous phenomena that can interest turbine structure affected by high thermal gradient is the creep.

- Steady pressure field, due to a different pressure field between Suction Side and Pressure Side of the blades. It can be expressed by the following equation:

$$F_p = \int pndS$$

Regarding dynamic loads, they can be divided into two main categories, based on their origin:

- Synchronous vibration, where the harmonic terms are function of the number of blades and angular velocity. These dynamic excitations are originated from unsteady pressure fields.
- A-synchronous vibration, where frequencies are not multiplies of rotation speed of the system. They are due to flux instability as separations, vortex shedding and rotor stall

Generally, pressure field is considered fixed in space and constant in time, but due to the presence of statoric sectors upstream and downstream the rotoric stage, pressure field cannot be axisymmetric. For synchronous vibration, the excitations frequency depends on the rotational speed according to the following relationship:

$$\omega = EO \cdot \Omega$$

EO stands for Engine Order and it denotes the periodicity of the excitation over the bladed disc. For a rotor, the Engine Order is given by the number of blades of the previous stator (and in this case the excitation is due to the stator wakes).

Forced response can be associated to:

- High EOs, due to the interaction between rotor and stator row
- Low EOs, due to high nodal diameters discontinuities, as unbalanced rotating masses, asymmetric shaft's supports, interaction with distorted flow.

Forced response is a harmonic function, so it can be written through Fourier series expansion:

$$F(\alpha) = F_0 + \sum_{eo} F_c^{eo} \cos(eo \cdot \alpha) + F_s^{eo} \sin(eo \cdot \alpha)$$
$$= F_0 + \sum_{eo} F^{eo} \cos(eo \cdot \alpha + \delta)$$

where $\alpha = \omega t$. When there is an engine order, the forces affecting two following sectors are out of phase each other by an angle $\psi = eo\frac{2\pi}{N}$. It can be defined a vector of forced response acting on all the disc, related to the engine order:

$$\{F_{eo}\} = \begin{Bmatrix} I_j \\ I_j e^{-i\psi} \\ \vdots \\ I_j e^{-i(n-1)\psi} \\ \vdots \\ I_j e^{-i(N-2)\psi} \\ I_j e^{-i(N-1)\psi} \end{Bmatrix} \{F^{eo}\}$$

The main excitation forces that contribute to the unsteadiness in the flow are the following:

- Viscous interaction, due to the generation of wakes.
- Potential interaction, due to field perturbations which are generated by the pressure variations due to the passing blades.
- Shock perturbations, due to the static pressure field changes. Their presence can create very localized unsteady pressure.
- Vortex shedding, a phenomenon which interests wide trailing edge turbine blades.

3.4.2 Campbell's Diagram

In order to study the forced response of a bladed disc, the most commonly used instrument is the *Campbell's Diagram*, provided by Wilfred Campbell. This graphical instrument is useful to find the presence of resonances, corresponding to the situations in which the frequency of the exciting force coincides with one of the natural frequencies of the system.

The natural frequencies are represented as a set of lines which are function of the rotation speed of the system. If, in first approximation, the stiffening effect of the centrifugal force on the blade modes is neglected, natural frequencies are given by horizontal lines.
Instead, the EO excitation frequencies are represented by straight lines starting from axis origin, according to the equation $\omega = EO \cdot \Omega$.

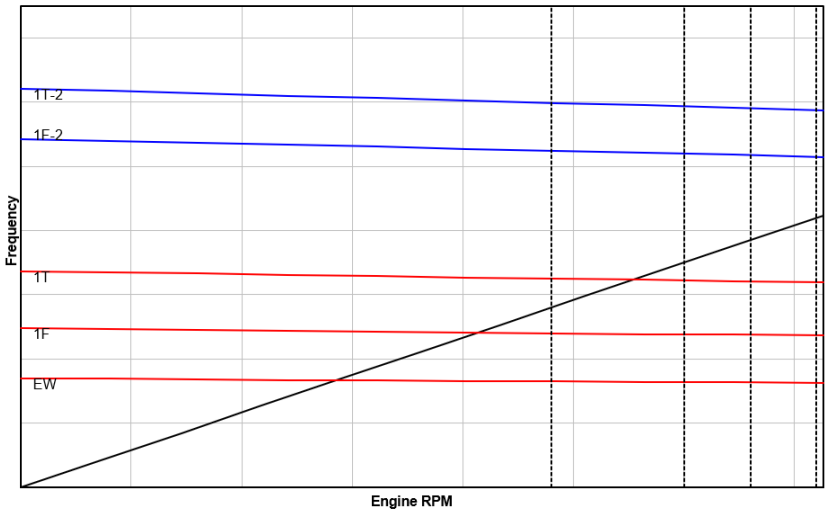

Figure 20: Example of Campbell's Diagram

A necessary but not sufficient condition to resonance occurs when excitants' lines cross the ones of natural frequencies. In a Campbell's diagram, the number of crossings between natural frequencies and excitation frequencies is usually very high, so the purpose is to verify which crossings represent resonance conditions.

The critical intersections are given by the following relation:

$$EO' = EO - k \cdot N = ND \quad \forall k \in \mathbb{N}$$

A graphical representation is given by the *Zig-Zag diagram*, with harmonic index on horizontal axis and engine order on the vertical one.

When $k = 0$ the EO equals the number of nodal diameters of the mode shape, which means that the force distribution over the structure exactly match the shape of the mode. Therefore, when natural frequency and excitation frequency are the same, the maximum response amplification is obtained. Instead, mode shapes such that $h \neq EO$ cannot excited in resonance condition because the modal force (which is the force projection onto the mode) is null.

When $k \neq 0$ the response of the structure is given by a new phenomenon called *aliasing*. Aliasing on a turbine is a phenomenon due to the discontinuity of the flow that invests the blades of a sector. The maximum value of nodal diameter is set by the stage number of blades, so any engine order that exceed this value is capable of exciting a blade's row thanks to the Aliasing phenomenon.

3.4.3 Low Engine Order (LEO) Forced Response

In a turbine stage, rotor blades are excited from the upstream stator wakes or flow disturbances. If the blades are not deformed in the stator ring, all the rotor blades are excited in a periodic way with same amplitude, which change in phase for each blade. The quickest way to identify forced response regions of a blade row is using the Campbell's Diagram, which shows crossing of excitation frequencies due to upstream and downstream vanes. In each crossing, there is the risk of a resonant excitation of the structure.

In practice, in the Campbell's Diagram, an additional line is added to indicate another excitation of low frequency, named the LEO excitation. This kind of excitation can be caused by non-uniformities on the stator blade row due to wear (as erosion or burnout). The presence of LEO excitations produces vibrations in blade modes such as the first bending or torsion made, which have low frequency and large vibration amplitudes. Due to the large increase in amplitude, this phenomenon may cause HCF (high cycle fatigue) failure.

LEO excitations are more difficult to predict then ones due to vane passing and the reasons are the following:

- Typically, the frequency and magnitude of a LEO excitation is caused by unknown variations in the vane geometry due to wear on the vanes during the component's life.
- Also, the periodicity of LEO excitation is not known a priori.

3.5 Modal shapes and Fre-ND diagram

The dynamics of a bladed disc can be described by the Fre-ND diagram, which represents the plot of natural frequencies versus the number of nodal diameters characterizing the associated mode shapes. The number of natural frequencies is given by the number of nodal diameters of the system.

The Fre-ND diagram shows the sector deformed shapes, which are grouped into distinct families of modes (whose number is equal to the number of DOFs). As the number of nodal diameters increases, the vibratory nature of the bladed disc affects the shape of each family because the disc becomes stiffer leading to growing natural frequencies. Fre-ND diagram is a symmetric plot, but negative nodal diameters are not conventionally represented. Watching the diagram below, it can be note that all modal families have a growing trend. Reaching a certain value of nodal diameter, the modal family approaches one asymptotical natural frequency, which is the one of the clamped, blade only configuration. In this case, the disc can be considered nearly motionless, and the blades are weakly coupled among themselves.

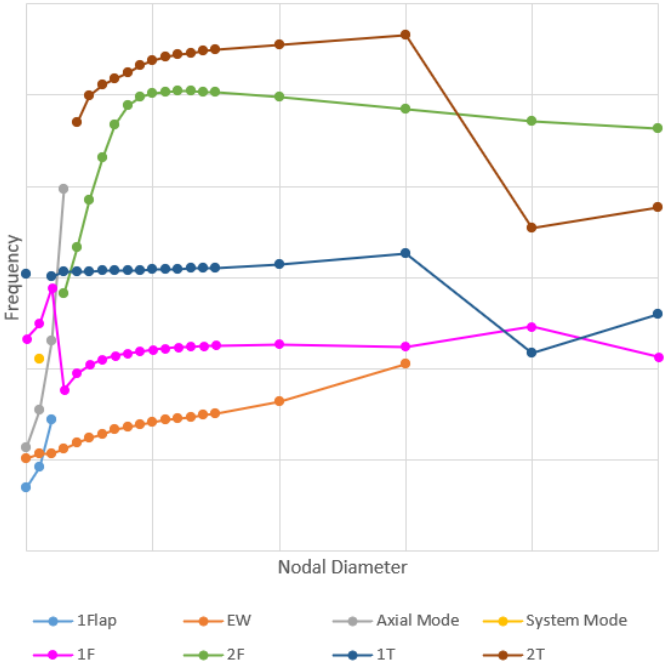

Figure 21: Example of a Fre-ND diagram

For low NDs, modal shapes are typically disc modes, where the greatest deformations occur at the disc, while the deformation of the blades can be considered negligible. Instead, for high NDs, they are called blade modes, where the disc is highly stiff, and the deformation occurs only on the blade.

In many cases, it is possible that two different modal families have similar natural frequencies, for a given nodal diameter, and this phenomenon is called veering. The veering zone is the approach point where the modal families exchange modes of vibration.

Another fundamental step for building a Fre-ND diagram is to classify the modal families. The most common bladed modes are the following:

- Edgewise (EW), when the blade's tip moves along the engine axis.
- Flapwise (FW), when the blade's tip moves along the tangential axis.
- Flexural bending (F) when maximum displacement is reached tangentially at half span.
- Torsional or Twist (T) when the blade twists around the radial axis.

Frequently, a mode can be given from the combination of more modal shapes. This is what happens when, increasing the modal family order, the vibrations become more and more complex, and they are described by the combination of flexion-torsional modes.

Modal shapes' nomenclature indicates the order and the number of half waves or couples of lobes of the deformed shape. For example, 1F indicated the first flexural bending with one half wave, 1F2 indicates the second flexural bending with one half wave and 2F indicates a flexural bending with two half waves.

3.6 Modal Assurance Criterion (MAC)

The Modal Assurance Criterion is a statical indicator which provide a measure of consistency (degree of linearity) between estimates of a modal vector. It provides an additional confidence factor in the evaluation of a modal vector from different excitation locations or different modal parameter estimation algorithms. This method was developed on the late 1970s from the need for a quality assurance indicator for experimental modal vectors in frequency response.

An important factor using to describe the modal assurance criterion is the ***modal scale factor (MSF)*****,** which function is to normalize all estimates of the same modal vector, considering magnitude and phase differences. When the two modal vector estimates have the same scale, their elements can be averaged, differenced, or sorted to provide a best estimate of the modal vector or to find the type of error vector overlapped on the modal vector. So, the modal scale factor is a normalized estimate of the modal participation factor between two modal vector estimates for a specific mode of vibration. It is defined as:

$$MSF = \frac{\{\psi_{cr}\}^T\{\psi'_{dr}\}}{\{\psi_{dr}\}^T\{\psi'_{dr}\}} \qquad or \qquad MSF = \frac{\sum_{q=1}^{N_0}\psi_{cqr}\psi'_{dqr}}{\sum_{q=1}^{N_0}\psi_{dqr}\psi'_{dqr}}$$

Where:

- $\{\psi_{cr}\}$ is modal vector for reference *c*, mode *r*.
- $\{\psi_{dr}\}$ is modal vector for reference *d*, more *r*.
- $\{\psi'_{cr}\}$ is complex conjugate of $\{\psi_{cr}\}$.
- $\{\psi'_{dr}\}$ is complex conjugate of $\{\psi_{dr}\}$.

- N_0 is the number of outputs.
- ψ_{cqr} is modal coefficient for reference *c*, degree of freedom q, mode *r*.
- ψ_{dqr} is modal coefficient for reference *d*, degree of freedom q, mode *r*.

For complex modes of vibration, it can be written as:

$$MSF = \frac{\{\psi_{dr}\}^H\{\psi'_{cr}\}}{\{\psi_{dr}\}^H\{\psi'_{dr}\}}$$

The modal scale factor and the modal assurance criterion also provide a method of comparing estimates of modal vectors which comes from different sources. For example, modal vectors from a finite element analysis can be compared with modal vectors determined experimentally, in order to evaluate the mutual consistency of different procedures. Furthermore, if some degrees of freedom could not be measured for an experimental modal vector, the analytical modal vector can be used to complete it.

The ***modal assurance criterion*** is defined as a scalar constant relating the degree of consistency between two modal vectors:

$$MAC = \frac{|\{\psi_{cr}\}^T\{\psi'_{dr}\}|^2}{\{\psi_{cr}\}^T\{\psi'_{cr}\}\{\psi_{dr}\}^T\{\psi'_{dr}\}} \quad or \quad MAC = \frac{|\sum_{q=1}^{N_0}\psi_{cqr}\psi'_{dqr}|^2}{\sum_{q=1}^{N_0}\psi_{cqr}\psi'_{cqr}\sum_{q=1}^{N_0}\psi_{dqr}\psi'_{dqr}}$$

The MAC's range values are from zero (no consistent correspondence) to one (consistent correspondence). The modal assurance criterion can only indicate consistency, not validity or orthogonality, therefore eventually invalid assumptions can be the cause of potential error.

$MAC = 0$ indicates that the modal vectors are not consistent, and the main reasons can be the following:

- System is not stationary.
- Presence of noise on the reference modal vector.
- Invalid modal parameter estimation.
- Modal vectors are from linearly unrelated mode shape vectors

$MAC = 1$ means that the modal vectors are consistent, but it is not a sufficient condition to say that they are correct. The main reasons of this results are the following:

- Modal vectors have been incompletely measured.
- Modal vectors are the result of an undesired forced excitation.
- Modal vectors are primarily coherent noise.
- Modal vectors represent the same modal vector with only different scaling. That's the situation in which the two vectors are corrects and they differ only by the complex valued scale factor.

Today, the results of modal assurance criterion can be plotted using color to represent magnitude.

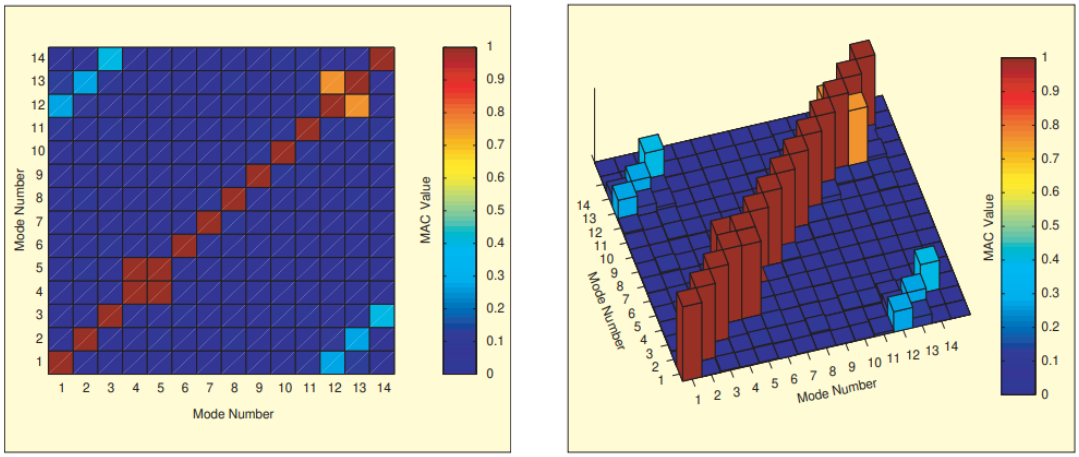

Figure 22: 2D and 3D representation of MAC values [8]

Chapter 4

Low Pressure Turbine (LPT)

Turbines are the most critical components of the engine due to the high temperatures of the exhaust gases coming from the combustion chamber. Their main function is to drive the compressor stages and the fan. Turbines may be classified into radial, axial, and mixed-flow machines (the latter is a combination of radial and axial motion of the fluid relative to the rotor). Axial turbines are the most common used in aeronautical field because they can handle greater mass flow and it is possible to obtain higher pressure ratios due to the multi-staging components. The mass flow must be as large as possible to minimize the drag and the engine weight, and it is limited by the maximum permissible Mach number of the flow entering the compressor. Turbine's efficiency is generally higher than the compressor's efficiency due to the fluid has a press drop rather than the pressure increases in the compressor. This fact prevents the detachment of the boundary layer fluid, so it is sufficient to avoid separation problems. In turbine stages, it is possible to obtain more turning in a blade row without flow separation and this has an impact on the efficiency of the engine. To drive the compressors and accessories, turbine consists of several stages that are divided into a row of stationary guide vanes (called nozzles) and a row of moving blades. The number of stages is given by the relationship between the power required from the flow, the shaft rotational speed and the diameter of turbine. Also, the number of shafts and turbines changes with the type of engine: for high compression ratio engines, the best configuration is the two shaft one, which divides the engine into a high and a low-pressure section, while for a high bypass ratio fan engine, it is preferred a triple-spool system.

Another important configuration is the free-power turbine, which allows the turbine to rotate at its optimum speed thanks to its independence from the other shafts. The main downside is the possible overspeed until the destruction after losing its connection to the propeller load, so the risks are slightly higher than a traditional configuration.

4.1 Axial turbine design

A typical axial turbine stage is divided into a row of stationary blades (nozzle) and a rotor. The nozzle and rotor blades have an increasing length due to the large pressure drop per stage, which permits to hold the axial velocity to a uniform value through the stage. The function of the nozzle is to accelerate the flow giving it an increased tangential velocity component, while the rotor gives a torque in the direction of motion, changing the tangential momentum of the fluid. The consequence is that the work is done by the fluid on the rotor.

Applying the equation of angular momentum for steady flow:

$$\sum \tau = \dot{m}(rc_\theta|_2 - rc_\theta|_3)$$

it is possible to define the power output as:

$$\dot{\mathcal{L}} = \dot{m}(U_2 c_{\theta 2} - U_3 c_{\theta 3})$$

As well known, in axial turbine the blade speed U is keeping constant through the sections, so the turbine work per unit mass can be expressed as:

$$\mathcal{L} = U(c_{\theta 2} - c_{\theta 3}) = c_p(T_{01} - T_{03}) = c_p \Delta T_0$$

The stage work ratio is given by:

$$\frac{\Delta T_0}{T_{01}} = \frac{U(c_{\theta 2} - c_{\theta 3})}{c_p T_{01}}$$

The aim of an engine design is to maximize the turbine work per stage because it has a great influence on the overall efficiency. To do this, the work can be limited following two different strategies:

- Limiting the available pressure ratio (i.e. $\frac{\Delta T_0}{T_{01}}$) , which consequence is that the maximum work will be directly proportional to the entering temperature T_{01}.
- Limiting the work by the allowable blade speed U and the allowable turning of the fluid Δc_θ. It is possible when the available pressure ratio is sufficiently high, so the first strategy is not suitable. The blade speed U depends on the allowable rotational stresses at the operating temperature, while the turning of the fluid Δc_θ is useful to keeping high efficiency.

Thanks to the falling pressure gradient, boundary layer does not tend to separate and the greater the acceleration in a blade row, the smaller the losses. However, locally there could be some zones of adverse gradient due to the falling pressure within a blade passage. The result is the formation of a separation region with negative effects on the efficiency. So, generally the performance of a turbine blade row is less sensitive to the boundary layer condition than a compressor one.

4.1.1 Degree of Reaction

Turbine stages can be divided into two main categories:

- Impulse stages, where the entire pressure drop occurs in the nozzle guide vanes. The flow is directed on the turbine blades, so an impulse force is generated due to the impact of the gas.
- Reaction stages, in which a fraction of the pressure drop takes place in the nozzle and the rest in the rotor. The nozzle guide vanes are designed to deflect the flow without reducing the pressure. So, in the blade passages, a reaction force is generated as the results of the expansion and acceleration of the flow.

To identify the type of stage, it can be introduced a new parameter useful to evaluate the performance of the turbine. This parameter is the *Degree of Reaction*, and it is defined as the fraction of overall enthalpy drop occurring in rotor.

$$R = \frac{h_2 - h_3}{h_1 - h_3}$$

Generally, there is not pure impulse or pure reaction turbine blades but a combination of them. $R = 0$ means an impulse stage, while $R = 0.5$ indicates that the enthalpy drop is equally distributed between the stator and the rotor.

The typical value of the degree of reaction is around 0.5 at the mean radius. In fact, the turbine blades are twisted which means that the gases expanding in the turbine do the same work along the length of the blade and the flow entering the exhaust system has a uniform axial velocity. The main consequence of this design choice is that the degree of reaction (but also temperature, velocity, and pressure) changes along the radius, which means that at the tip there will be values of $R > 0.5$, while at the root $R < 0.5$. A value of $R = 0.5$ means also that the velocity triangle is symmetric at the mean radius.

At the root, where the values of R are low, the pressure drop is higher but also the losses are great. Often the first turbine stage has $R = 0$ and the reason is that the following stages will be less thermally stressed. At the nozzle exit, the velocity can be supersonic, so the leading edge of the blades is pointed. Instead, at the tip there are high values of R, which means that the highest velocities are reached in the rotor.

The flow exit angle does not usually coincide with the blade exit angle, but there is a deviation angle, which depends on the geometry of the stage. When the nozzle is chocked, the supersonic expansion will alter the flow direction as long as the exit pressure is sufficiently low.

4.1.2 Main components

The main components of a turbine can be reassumed in:

- Nozzle guide vanes, characterized by an airfoil shape and located in the turbine casing to allow the expansion. The passage between following vanes is a convergent duct. They have usually a hollow form and they can be cooled by passing compressor delivery air through them. Cooling is such important because reduces the effects of thermal stress and its consequence deformation. The materials used for nozzle guide vanes are typical nickel alloys, due to heat resistance requested.
- Turbine discs, obtained from a machined forging. They can be built with an integral shaft or with a flange on which the shaft will be bolted. The discs are affected by large rotational stresses, and they operate in a cool environment. For these reasons, the resistance to

fatigue cracking has the greatest impact on the useful disc life. Today they are made in nickel alloys.

- Turbine blades, which are designed to provide passages between adjacent blades that provide an acceleration of the flow up to the smallest area (the throat). To obtain high efficiency, thin trailing edges are required in each section. There is a gap between blade tips and casing, which changes in size according to the thermal expansion or contraction. Instead of this configuration, a shroud is often fitted at the blade tip to reduce the loss of efficiency. The blades must carry the centrifugal loads due to the high rotational speed. Also, they must be resistant to fatigue and thermal shock, as high cycle fatigue (HCF) conditions. Another phenomenon that interests turbine blades is the creep, due to the elevated temperatures deformations. The accumulation of such deformation leads to fracture by a creep rupture mechanism, and it is the main cause of blade life reduction.

4.2 Efficiency

In a turbine stage, the aerodynamic losses depend on the degree of reaction. High values of degree of reaction allow to improve efficiency due to the less work per stage which means a larger number of stages. To control these losses, it is essential to understand aerodynamic phenomena and to find new methods to control the interaction between tip and outer casing wall.

Defining an ideal expansion reversible, it is possible to relate it with the real expansion through an empirical efficiency.

There are two different ways to define turbine efficiency and the choice depends on the engine in which the turbine is employed. In many conventional applications, the shaft power is the useful turbine output while the exhaust kinetic energy (in the figure 34 it is indicated as $\frac{c_3^2}{2}$) is considered a loss because it is not reused in the thermodynamic cycle, but it is only discharged outside. In this case, the ideal turbine is considered an isentropic machine without exhaust kinetic energy and the ideal turbine work can be expressed as:

$$W_{T,ideal} = c_p(T_{01} - T_{3s})$$

Comparing the actual turbine work with the ideal work means that the considering efficiency is the, so called, *total-to-static (TTS) turbine efficiency*. The reason of

this name is that the ideal work is based on total inlet conditions and static exit pressure.

$$\eta_{ts} = \frac{T_{01} - T_{03}}{T_{01} - T_{3S}} = \frac{1 - \frac{T_{03}}{T_{01}}}{1 - \left(\frac{p_3}{p_{01}}\right)^{\frac{\gamma-1}{\gamma}}}$$

In other applications, such as in turbojet engines, the exhaust kinetic energy is considered in the useful work of the turbine due to the high velocity exit of the exhaust gases. The new ideal work is:

$$W_{T,ideal} = c_p(T_{01} - T_{03s})$$

As the previous case, it is possible to introduce a *total-to-total (TTT) turbine efficiency*, which can be expressed as:

$$\eta_{tt} = \frac{T_{01} - T_{03}}{T_{01} - T_{03s}} = \frac{1 - \frac{T_{03}}{T_{01}}}{1 - \left(\frac{p_{03}}{p_{01}}\right)^{\frac{\gamma-1}{\gamma}}}$$

Comparing the two efficiencies, it is possible to notice that one of them is higher than the other one.

$$\eta_{tt} > \eta_{ts}$$

The reason takes place in the different efficiency definitions because the energy due to the tangential component of the exhaust velocity is a loss since it does not give any contribution to the thrust.

Chapter 5

Aeroelasticity

In the aerospace field it is important to know how aerodynamic forces affect performance and structure integrity. For studying phenomenology like flutter or forced vibration, we need to study the aeroelasticity interaction and its effects on turbomachinery in high fatigue cycle failures.

5.1 What is aeroelasticity

Aeroelasticity is the discipline that study the mutual interaction between solid structures and fluid flow. The nature of this field is illustrated by Professor Collar in the 1940s by his Collar's triangle. The triangle describes the interaction among:

- Aerodynamics, that explain the forces affecting on a body of a given shape
- Dynamics, that consider the effects of inertial forces acting on the body
- Elasticity, that predicted the forces acting on a body of a given shape

The study of all the three discipline is essential in solving aeroelasticity problems. The interaction between aerodynamics and dynamics affects the field of flight mechanics. In the Collar's triangle there are 4 regions of interaction:

- Flight mechanics, that studies trajectories and flow motion that the aircraft developed under the action of aerodynamics, propulsive and inertial forces

- Static aeroelasticity, which studies the interaction of aerodynamic loading induced by steady flow and the resulting elastic deformation of the lifting-surface structure
- Dynamic aeroelasticity, especially the instability called flutter, which can lead to a catastrophic structural failure
- Structural dynamics, which includes the determination of natural frequencies and mode shapes (free-vibration response), response due to initial conditions, forced response in the time domain and frequency response

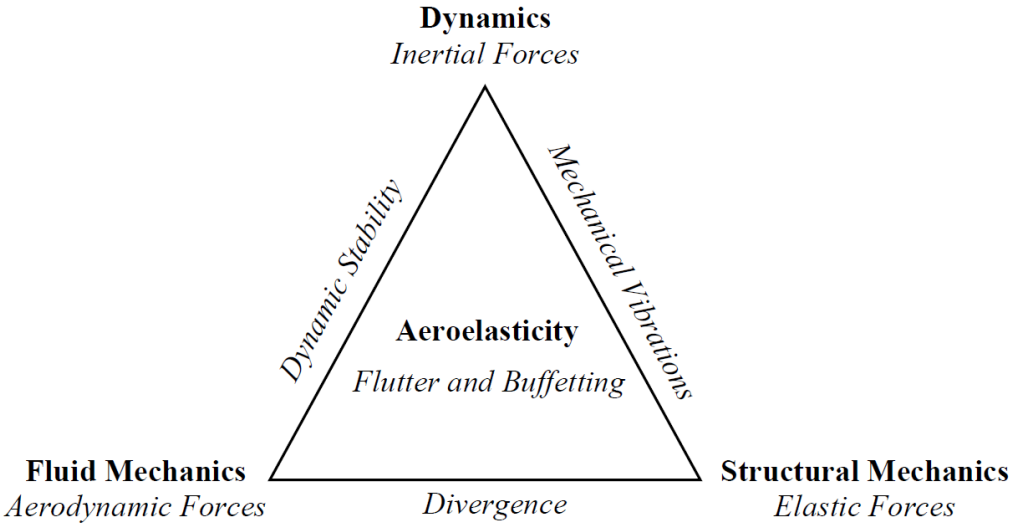

Figure 23: Collar's triangle [14]

The meaning of the Collar's triangle is to have a global vision of the problem because the various disciplines tend to mix with each other. For example, the load on a structure depends on the deformation and the deformation depends on the loads, so the aeroelastic problems are not linear, but they depend on several variables.

In the past, there is not knowledge about aeroelastic phenomena, and it led to catastrophic failure of the wings caused by their overloaded. The first documented case of flutter happened in 1916 and involved a dynamic twisting of the fuselage. Also, during the two World War there were many crashes due to aircraft flutter. Today the flutter may strongly affect the performance of an aircraft, positively or negatively, but it is always present during the life of a component.

Chapter 6

Reduced Order Model Techniques

6.1 Introduction

The finite element (FE) dynamic analysis of a structural system is often impracticable due to the large number of DOFs involved in the simulations (a FE model can consist of hundreds of thousands DOFs). So, it is more convenient to perform separate FE analysis on several substructures, which are generally designed independently to each other. Modern reduction techniques, like ones implemented on Policontact, are based on the concept of *dynamic substructuring* (DS) where the structure is decomposed into several substructures, which dynamic response is easier to evaluate. The dynamic models of these substructures are then assembled to obtain the complete dynamic model.

The main advantages of using this approach are reassumed in the following five points:

1) It allows the evaluation of large or complex structures that cannot be simulated as a single model.
2) Decomposing the structures into many subsystems, local dynamic behavior can be easily recognized during the analysis of each one. Also, it permits local optimization and simplification of the design, by eliminating local subsystem behavior with a negligible impact on the dynamics.
3) It allows to combine numerically and experimentally components.
4) For the substitution of a component, it does not compromise the entire model, but it requires only that component to be reanalyzed.

5) In a working group, it allows sharing and combining different component models design.

Only the decomposition of the model is not enough for the dynamic analysis, so it is necessary to decrease the number of DOFs involved. The dynamic substructuring methods described in the next chapters are based on the combination between concepts of analysis and model order reduction. In these methods, the dynamic of a FE model is described in terms of dominant mode shape vectors which represents the modal DOFs instead of physical DOFs. In this way, it is possible to compress the calculation times while maintaining structure mesh intact.

The first step for the creation of a substructured dynamic model is the decomposition of the structure into several components, non-overlapping each other. Next, the FE models of each component are created but it is necessary to decrease the number of DOFs without changing the mesh, as mentioned before. Using model order reduction methods, the structure's dynamic behavior will be expressed in terms of a limited number of deformation shapes with associated amplitudes. These methods do this building a reduction basis which collects the mode shape vectors that described the dynamic behavior of the component. It is possible to identify two main categories of modal order reduction methos:

- Component Mode Synthesis (CMS) methods
- Generalized modal reduction

In this thesis only the CMS methods will be treated, as they are used by the software Policontact.

6.2 Component Mode Synthesis (CMS)

In CMS methods, the transformation matrix R is a component-mode matrix and includes the following modes:

- Normal or vibration modes to describe the component's dynamics.
- Static modes referred to the interaction with adjacent substructures.

The motion equation for describing the linear dynamic behavior of the generic component is:

$$M^c \ddot{x}^c(t) + K^c \dot{x}^c(t) = f^c(t)$$

For each component there are three categories of DOFs:

- Interface DOFs, which include the DOFs shared with adjacent substructures. (x_i)
- Interior or exceeding DOFs, which include the DOFs not shared with the other substructures. (x_e)
- Accessories or active DOFs, used either to apply forces on the substructure or to evaluate its response. (x_a)

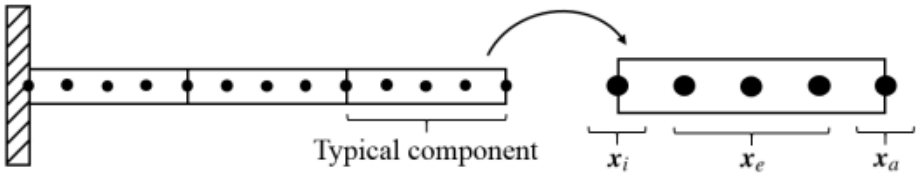

Figure 24: Example of DOFs partitioning of a typical substructure [24]

It is possible to define a boundary set which collects interface and active DOFs and it is defined as:

$$x_b = \begin{Bmatrix} x_a \\ x_i \end{Bmatrix}$$

Using this set, the previous equation can be rewritten in matrix form as:

$$\begin{bmatrix} M_{bb} & M_{be} \\ M_{eb} & M_{ee} \end{bmatrix} \begin{Bmatrix} \ddot{x}_b \\ \ddot{x}_e \end{Bmatrix} + \begin{bmatrix} K_{bb} & K_{be} \\ K_{eb} & K_{ee} \end{bmatrix} \begin{Bmatrix} x_b \\ x_e \end{Bmatrix} = \begin{Bmatrix} f_b \\ f_e \end{Bmatrix}$$

The interior DOFs response can be divided into its static and dynamic parts, as:

$$x_e = x_e^s + x_e^d$$

Imposing accelerations null and remembering that dynamic forces are not applied on the internal nodes, the static response is given by:

$$\begin{bmatrix} K_{bb} & K_{be} \\ K_{eb} & K_{ee} \end{bmatrix} \begin{Bmatrix} x_b \\ x_e^s \end{Bmatrix} = \begin{Bmatrix} f_b \\ 0 \end{Bmatrix}$$

$$x_e^s = -K_{ee}^{-1} K_{eb} x_b = \Psi_{eb} x_b$$

While the dynamic part can be approximated by the summation of vibration modes (n_v):

$$x_e^d \approx \sum_{j=1}^{nv} \phi_{e,j}\, n_j = \Phi_v n_v$$

where $\phi_{e,j}$ represent the vibration modes, obtained by solving the eigenvalue problem for the DOFs in x_e:

$$\left(K_{ee} - \omega_{e,j}^2 M_{ee}\right)\phi_{e,j} = 0$$

The final equation of the interior DOFs response can be expresses as:

$$x_e \approx \Psi_{eb} \cdot x_b + \Phi_v n_v$$

where x_e and x_b are the "slave" and "master" DOFs respectively. Managing the previous equations, the global component's displacements vector is given by:

$$x = \begin{Bmatrix} x_b \\ x_e \end{Bmatrix} \approx \begin{bmatrix} I_{bb} & 0 \\ \Psi_{eb} & \Phi_v \end{bmatrix} \begin{Bmatrix} x_b \\ n_v \end{Bmatrix} = Rq$$

where *R* is the transformation matrix while *q* is the generalized coordinates vector. Introducing the residual *r* into the component's motion equation, it can be obtained the following expression:

$$MR\ddot{q} + KRq = f + r$$

Multiplying both sides by R^T, the expression becomes

$$R^T MR\ddot{q} + R^T KRq = R^T f + R^T r$$

Remembering Galerkin's projection, i.e. $R^T r = 0$, the reduced component's motion equation is:

$$\tilde{M}\ddot{q} + \tilde{K}q = \tilde{f}$$

Due to the reduction of the number of DOFs, the new component model is stiffer than the full model, so the eigenfrequencies will be higher. Data recovery is the procedure which allows to expand the results of the analysis performed on the reduced model in order to obtain the solution at the original set of DOFs. The CMS methods differ from each other for the nature of the modes constituting the reduction basis *R*.

The software Policontact uses two CMS techniques, which are then combined through Tran's method. These methods are the Guyan reduction and the Craig-Bampton CMS, which will be described in the next chapters.

6.3 Guyan reduction

The Guyan reduction is a reduction method proposed in 1965 and it is still used today for dynamic analysis of complex structures. In this method, the transformation is applied to the mass matrix, based on partitioning the stiffness matrix and it neglects the inertia effect for the DOFs to be neglected. Guyan reduction is a static reduction as it involves only the matrix Ψ_{eb} neglecting the effect od modal DOFs. This method condenses the set x_e to the boundary DOFs using static constraint modes:

$$x_e = \Psi_{eb} x_b$$

The response of internal nodes is described as a function of the vector x_b which includes the accessories DOFs and the blade interface DOFs. Ψ_{eb} is the static condensation matrix or Guyan matrix.

$$x_e \rightarrow \text{ slave} \qquad x_b \rightarrow \text{ master}$$

So, in the reduction models, the slave vector x_e depends on the master vector x_b. Master DOFs mostly consist of contact interface, excitation and preload application and accessories DOFs to record the responses. All the others are considered slave DOFs. The Guyan coordinate transformation can be expressed as:

$$x = \begin{Bmatrix} x_b \\ x_e \end{Bmatrix} \approx \begin{bmatrix} I_{bb} \\ \Psi_{eb} \end{bmatrix} x_b = \Psi_{Nb} x_b = R_G x_b$$

The columns of the Guyan component-mode matrix R_G consists of static constraint modes only. The reduced system of equation is the following:

$$M_G \ddot{x}_b + K_G x_b = f_G$$

where M_G and K_G are the Guyan condensed mass and stiffness matrices respectively, while f_G is the condensed vector of generalized forces. They are defined as:

$$M_G = R_G^T M R_G = M_{bb} - K_{be} K_{ee}^{-1} M_{eb} - M_{be} K_{ee}^{-1} K_{eb} + K_{be} K_{ee}^{-1} M_{ee} K_{ee} K_{eb}$$

$$K_G = R_G^T K R_G = K_{bb} - K_{be} K_{ee}^{-1} K_{eb}$$

$$f_G = R_G^T f = f_b - K_{be} K_{ee}^{-1} f_e$$

The main Guyan assumption is that the inertial forces are condensed into the master vector x_b, so the exact solution is found if this method is applied to static problems. For dynamic problems, the exact solution is valid if the highest eigenfrequency is much lower than the lowest eigenfrequency of the substructure clamped as its interface. It means that the system vibrates too slowly to be able to appreciate dynamic phenomena and the response is predominantly static. This is due to the internal inertia forces which are statically condensed on the boundary.

The accuracy of the Guyan method depends on the number of DOFs neglected in the reduction problem. For obtaining a best reduction it is necessary to do the following steps:

- Include in the master vector x_b the nodes with the greatest mass.
- Include in the master nodes which gives a more relevant contribute in terms of kinetic energy and dissipated energy.
- Evenly distribute the nodes along the structure.
- Include the nodes affected by an external force.

6.4 Craig-Bampton Component Mode Synthesis (CB-CMS)

It is a reduced order modelling technique for a generic system with a friction contact. An efficient ROM can be performed to condense the system to a small set of DOFs without lose the dynamic properties of the structure. The resulting small system is more efficient to compute the non-linear dynamic response of the system.

This reduced order model is an expansion of the Guyan Method that include information on the internal dynamics in the reduced component model. This advantage can be obtained by expanding the reduction basis with fixed-interface vibration modes. The main consequence is a completer and more versatile basis to describe the component's dynamic behavior.

For a structure with friction contact interface, the equation of motion is:

$$M\ddot{x}(t) + C\dot{x}(t) + Kx(t) = f_e(t) - f_{nl}(x, \dot{x}, t)$$

where:

- M, C, K are the reduces mass, damping and stiffness matrices respectively.
- x is the reduced vector of DOFs.
- f_e and f_{nl} are the corresponding vectors of the external and non-linear contact forces.

The homogeneous undamped linear system is given by the following equation:

$$M\ddot{x}(t) + Kx(t) = 0$$

The DOFs of the system are partitioned into boundary and interior DOFs, so the equation of motion can be approximated as:

$$x_e \approx \Psi_{ee} x_b + \Phi_{ek} \eta_k$$

Also in this reduction method, the DOFs are divided into master and slave DOFs, where the master DOFs are the boundary DOFs. In Craig-Bampton method, only master DOFs are included in the reduced model as physical DOFs, while the slave DOFs are replaced by modal DOFs η_k.

$$x = \begin{Bmatrix} x_b \\ x_e \end{Bmatrix} \approx \begin{bmatrix} I_{bb} & 0 \\ \Psi_{eb} & \Phi_{ek} \end{bmatrix} \begin{Bmatrix} x_b \\ \eta_k \end{Bmatrix} = R_{CB} x_{CB}$$

R_{CB} is the CB-CMS component-mode matrix or reduction matrix. Ψ_{eb} contains the static constraint modes while Φ_{ek} is the fixed interface normal mode shapes constrained at the master DOFs. Using the reduction matrix R_{CB}, the reduced equations of motion:

$$\begin{bmatrix} \widetilde{M}_{bb} & \widetilde{M}_{bk} \\ \widetilde{M}_{kb} & I \end{bmatrix} \begin{Bmatrix} \ddot{x}_b \\ \ddot{\eta}_k \end{Bmatrix} + \begin{bmatrix} \widetilde{K}_{bb} & 0 \\ 0 & \Omega_{kk}^2 \end{bmatrix} \begin{Bmatrix} x_b \\ \eta_k \end{Bmatrix} = \begin{Bmatrix} \tilde{f}_b \\ \tilde{f}_k \end{Bmatrix}$$

where:

$$\widetilde{M}_{bb} = M_{bb} - M_{be}K_{ee}^{-1}M_{eb} - K_{be}K_{ee}^{-1}M_{eb} + K_{be}K_{ee}^{-1}M_{ee}K_{ee}^{-1}K_{eb}$$

$$\widetilde{K}_{bb} = K_{bb} - K_{be}K_{ee}^{-1}K_{eb}$$

$$M_{kb} = M_{bk}^T = \Phi_{ek}^T(M_{eb} - M_{ee}K_{ee}^{-1}K_{eb})$$

$$\tilde{f}_b = f_b - K_{be}K_{ee}^{-1}f_e$$

$$\tilde{f}_k = \Phi_{ek}^T f_e$$

Ω_{kk}^2 is the diagonal matrix which contains the first η_k fixed interface eigenfrequencies ω_{ej}^2. This set of reduced matrix represents the reduced model, and it can be used to perform the nonlinear analysis. The accuracy of the results depends on if there are enough normal modes in the reduced system.

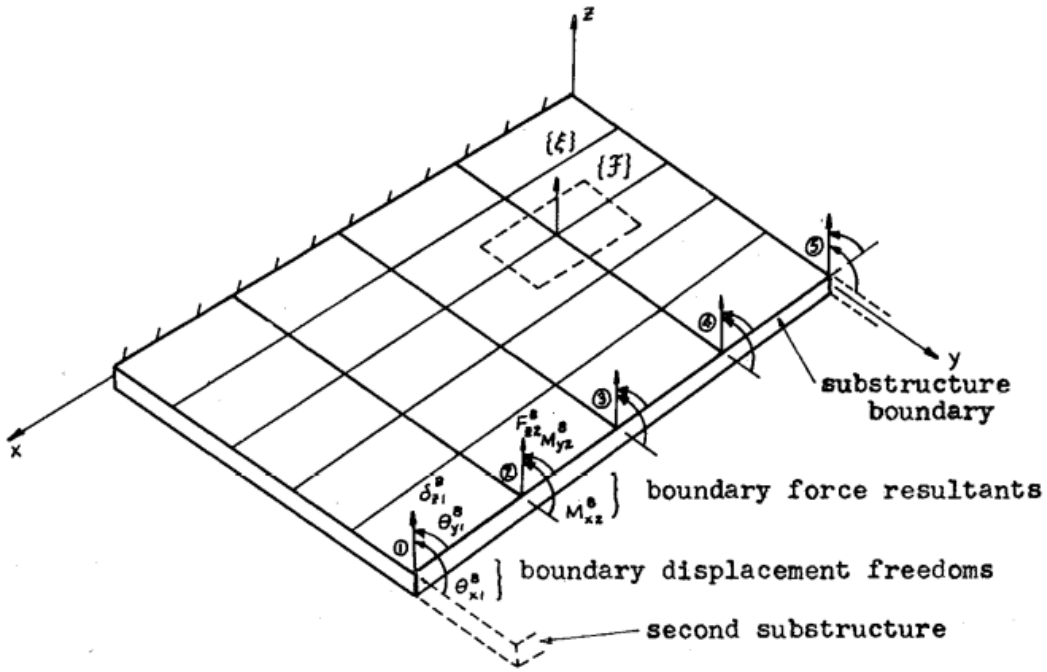

Figure 25: Example of CB-CMS reduction with the original substructure coordinates and the substructure boundary displacement coordinates [28]

6.5 Tran method

The Train method is a reduction technique developed by Tran in [33] for cyclic symmetric structures. For this kind of structures, performing analysis on FE models of only the fundamental sectors is computationally convenient, but it is not sufficient to reduce the size of the dynamic problem. So, the advantage of this technique is the combination between cyclic symmetry constraints and CMS methods to obtain highly reduced models.

Tran method is used to further reduce the master DOFs remained after the CB-CMS reduction and, in particular, it reduces the interface DOFs replacing them

with a linear combination of modal shapes. So, an important reduction of the independent frontier of a sector can be performed by this method.

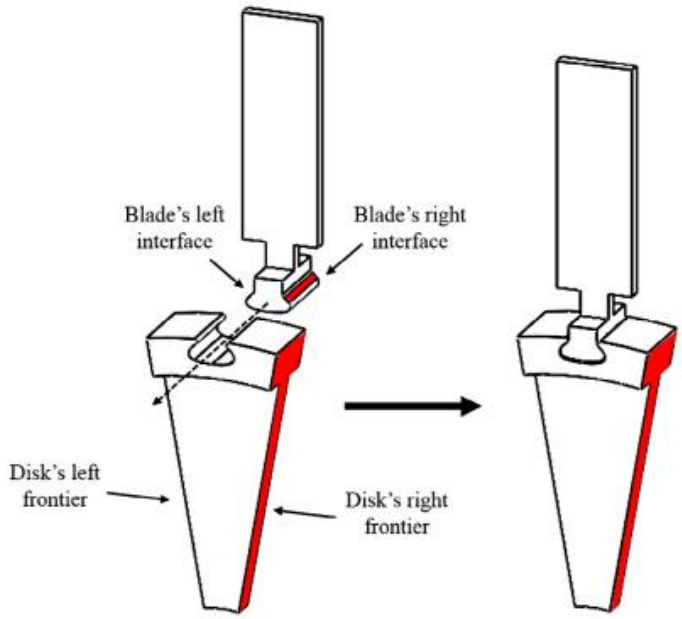

Figure 26: Example of a dummy blade attached to the fundamental sector [24]

The new partition of the DOFs of the fundamental sector is:

$$x_s = \begin{Bmatrix} x_b \\ x_e \end{Bmatrix} = \begin{Bmatrix} x_a \\ x_l \\ x_r \\ x_e \end{Bmatrix}$$

where a means active, l means left frontier, r means right frontier and e are the exceeding DOFs. Using the CB-CMS coordinate transformation, the sector's reduced vector is:

$$\begin{Bmatrix} x_b \\ x_e \end{Bmatrix} \approx \begin{bmatrix} I_{bb} & 0 \\ \Psi_{eb} & \Phi_{ek} \end{bmatrix} \begin{Bmatrix} x_b \\ \eta_k \end{Bmatrix} = R_{CB} x_{CB}$$

If the CB-CMS reduction retains the physical DOFs at the left and right frontier, the coordinates of right frontier x_r can be expressed in terms of the coordinates of left frontier x_l through the cyclic constraints. The reason is that cyclic symmetric structures typically have a response characterized by waveforms under the action of a wave EO excitation and the number of waves equals the number of nodal

diameters of the excited mode shape. The consequence is a phase delay φ_h in the motion between the left and right frontier. The new set of equation is the following:

$$x_{CB} = \begin{Bmatrix} x_b \\ x_e \end{Bmatrix} = \begin{Bmatrix} x_a \\ x_l \\ x_r \\ x_e \end{Bmatrix} = \begin{bmatrix} I & 0 & 0 \\ 0 & I & 0 \\ 0 & Ie^{i\varphi_h} & 0 \\ 0 & 0 & I \end{bmatrix} \begin{Bmatrix} x_a^h \\ x_l^h \\ \eta_k^h \end{Bmatrix} = T_{CB,CS}^h x_{CB,CS}^h$$

Now, it is necessary to build a new Guyan reduction order model keeping only the left and right frontiers DOFs as master. So, the frontier DOFs x_l and x_r are grouped into the set of interface DOFs x_i and the Guyan reduced order model is obtained by using the following coordinates transformation:

$$x_s = \begin{Bmatrix} x_l \\ x_r \\ x_e \end{Bmatrix} = \begin{Bmatrix} x_i \\ x_e \end{Bmatrix} \approx \begin{bmatrix} I_{ie} \\ \Psi_{ee} \end{bmatrix} x_i = \Psi_c x_i = R_G x_i$$

From the previous system, it is possible to obtain the Guyan condensed mass and stiffness matrices. Using the cyclic constraints, the right frontier DOFs can be expressed in terms of left frontier DOFs as following:

$$x_i = \begin{Bmatrix} x_l \\ x_r \end{Bmatrix} = \begin{bmatrix} I \\ Ie^{i\varphi_h} \end{bmatrix} x_l^h = R_{G,CS}^h x_l^h$$

By projecting the Guyan motion equation onto the basis $R_{G,cs}^h$, it is possible to obtain the following cyclic motion equation:

$$M_{G,cs}\ddot{x}_l^h + K_{G,cs}x_l^h = f_{G,cs}$$

The lowest eigenfrequencies eigenvectors can be founded by solving the following eigenproblem:

$$\left(K_{G,cs} - \omega_j^2 M_{G,cs}\right)\phi_j = 0 \qquad \forall j = 1, \dots, n_l$$

and they allow to reduce the independent frontier x_l^h through the interface modes. Arranging a subset of n_u interface mode as the columns of the matrix Φ_{lu}^h, the array x_{CB}^h can be reduced as:

$$x_{CB}^h = \begin{Bmatrix} x_a^h \\ x_l^h \\ \eta_k^h \end{Bmatrix} \approx \begin{bmatrix} I & 0 & 0 \\ 0 & \Phi_{lu}^h & 0 \\ 0 & 0 & I \end{bmatrix} \begin{Bmatrix} x_a^h \\ \eta_u^h \\ \eta_k^h \end{Bmatrix} = \begin{bmatrix} I & 0 & 0 \\ 0 & \Phi_{lu}^h & 0 \\ 0 & 0 & I \end{bmatrix} x_T^h$$

The vector x_T^h represents the *Tran generalized coordinate vector* and the Tran coordinated transformation is clearly effective when $n_u \ll n_l$.

Tran method computes the modes ϕ_j at the left frontier without separate them from the active ones, that is typical of the GSI reduction technique. The main disadvantage of the Tran method is that requires two reductions of the original FE model, so it is more computationally expensive than the GSI method.

6.6 Modal reduction

The modal transformation matrix is defined for a given system of *n* DOFs as:

$$[\Psi] = [\{\psi_1\} \quad \cdots \quad \{\psi_n\}]$$

ψ_i is the i-th eigenvector. The motion equation can be written in the modal domain approximating physic displacements with a linear combination of a limited number of modes, applying the modal superimposition principle:

$$\{x\} \approx [\Psi]\{q\}$$

$\{q\}$ is defined as the modal DOFs of the system, while $[\Psi]$ is the modal basis. Using this formulation, it is possible to rewrite the mass, stiffness and damping matrices which compare into the motion equation:

$$[M_{mod}] = [\Psi]^T[M][\Psi]$$

$$[C_{mod}] = [\Psi]^T[C][\Psi]$$

$$[K_{mod}] = [\Psi]^T[K][\Psi]$$

$$[F_{mod}] = [\Psi]^T[F]$$

The main benefit of this operation is the reduction of the computational cost to solve the system. Using N for the number of DOFs of the model and n for the number of modal shapes used in the reduction, the modal matrices size is $n \times n$

and they are square and diagonal, while the previous matrices size is $N \times N$. The motion equation becomes:

$$[M_{mod}]\{\ddot{q}\} + [C_{mod}]\{\dot{q}\} + [K_{mod}]\{q\} = \{F_{mod}\}$$

where:

$$[M_{mod}] = [I]$$

$$[C_{mod}] = \begin{bmatrix} 2\zeta_1\omega_1 & 0 & 0 \\ 0 & \ddots & 0 \\ 0 & 0 & 2\zeta_n\omega_n \end{bmatrix}$$

$$[K_{mod}] = \begin{bmatrix} \omega_1^2 & 0 & 0 \\ 0 & \ddots & 0 \\ 0 & 0 & \omega_n^2 \end{bmatrix}$$

The terms ζ and ω are the modal damping and the natural frequencies of the system respectively. The system defined above can be reduced assuming that, for a specific condition, only a limited subset of modes participate significantly to the motion, so the others can be neglected. The consequence is that for a given system of n DOFs in which $n - m$ modes are neglected, the modal transformation matrix becomes:

$$[\Psi'] = [\{\psi_1\} \quad \cdots \quad \{\psi_m\}]$$

Using this new transformation matrix, the coordinates can be approximated in this way:

$$\{x\} = [\Psi]\{\eta\} \rightarrow \{x\} \approx [\Psi']\{\eta\}$$

Now, the modal system becomes:

$$[M_{red}]\{\ddot{\eta}\} + [K_{red}]\{\eta\} = [\Psi']^T\{F\}$$

$[M_{red}]$ and $[K_{red}]$ are still diagonal matrices composed by modal mass and stiffness respectively, so this means that neglecting modes does not change diagonality of the matrices due to the transformation.

Modal reduction is a simplified approach, so it leads two main sources of errors:

- Not consider the neglected $n - m$ modes.

- Neglected the modal coupling due to damping. In fact, if it is considered the hypothesis of not proportional damping, the damping modal matrix is not diagonal.

Chapter 7

Approach

In this section, an introduction about LPT blades and the approach used in this thesis project are introduced and described. The goal is to give an overview about the main steps followed during this thesis work.

7.1 LPT Blade

An LPT (lower pressure turbine) blade is made up by:

- Shank (divided into upper shank and dovetail)
- Airfoil
- Shroud

The shank is the lower part of the blade which is in contact with the disk. The dovetail is the lower part of the shank.

Airfoil is the section blade where aerodynamic forces produce the motion of the blade, and the shape of airfoil is the most expensive part to project.

The shroud is the upper part of the blade.

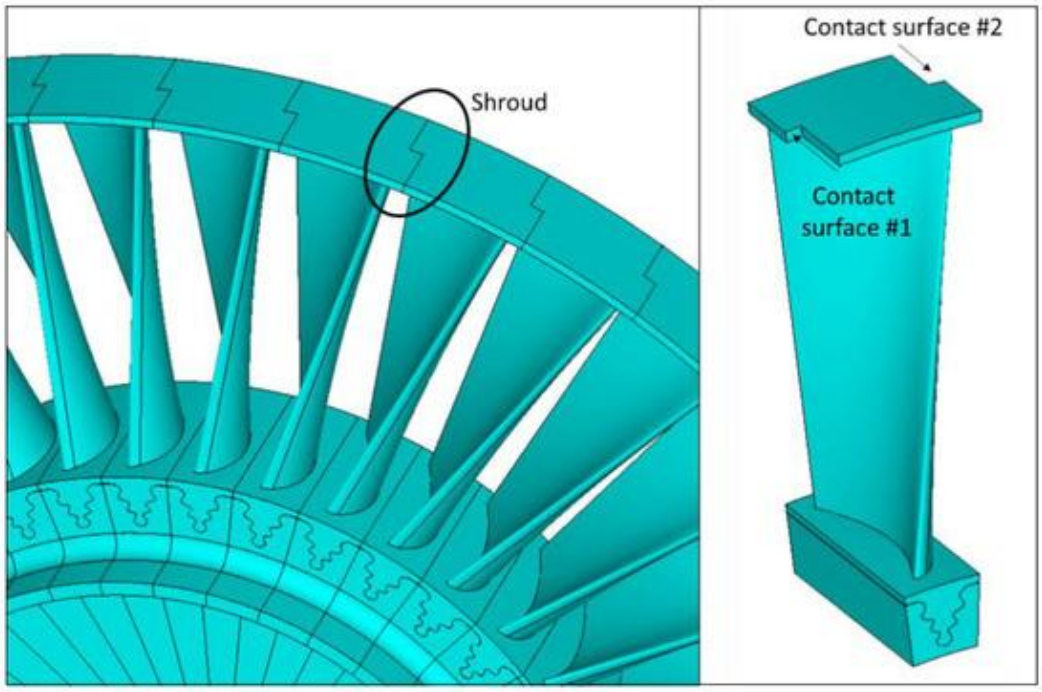

Figure 27: Shrouded blades [34]

This thesis project is based on the study of the interlocking behavior, in particular the impact of interlocking angle on wear behavior and forced response analyses.

The interlocking is the contact surface between two consecutive blades at the tip shroud, so it is the region where motion is transmitted from one blade to another. In this contact region, an excessive wear impact can cause resonance condition which concludes with HCF failure. This behavior is due to the removed volume at the interlocking interface, which can change the mode shapes of the blades into a tip free condition.

The main goal of this thesis project is to study the influence of interlocking angle on forced response analyses (FRA) and wear behavior, in order to avoid HCF failure.

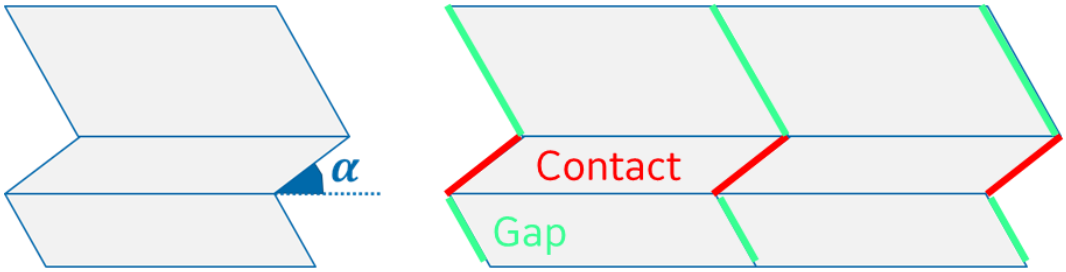

Figure 28: Interlocking angle α

Figure 29: Interlocking is located at the tip shroud [35]

7.2 Workflow

In this subsection, the thesis workflow followed to obtain the final results is explained. The first step is to analyze finite element models (FEM) and to run Modal and Static analyses.

From Modal analyses, it is possible to recognize modal shapes and to build Fre-ND diagram, in which every modal shape is represented as a function of frequency and nodal diameter. Modal recognition is important to understand the dynamic behavior of the blade.

After modal recognition, modal shapes are known and classified so it is possible to study the Campbell diagram, in order to find any possible crossing along the

operative range of the engine. Crossing identification is done for a specific engine order, who is important for the study of the engine.

From Static analyses, combining the results from Campbell diagram, it is possible to build the Goodman diagram. Goodman diagram represents the action of dynamic and static stress acting on the blade. Its function is to identify the critical location of the blade, which is located on the Haigh's curve. After the identification of Critical area, it is possible to identify the Critical dynamic stress.

Critical dynamic stress is used to find the gas load force unknown in linear forced response analyses (FRA). This unknown force is represented by the force that reach the critical dynamic stress in the critical location.

After linear FRA, it is important to study the effects of the non-linear contact at the interlocking interface by studying non-linear forced response analyses. Doing a sensitivity on the contact preload, it is possible to build the performance curve of the blade.

At the end, wear analyses are done for a wear evaluation about the behavior of interlocking interface for several cycles.

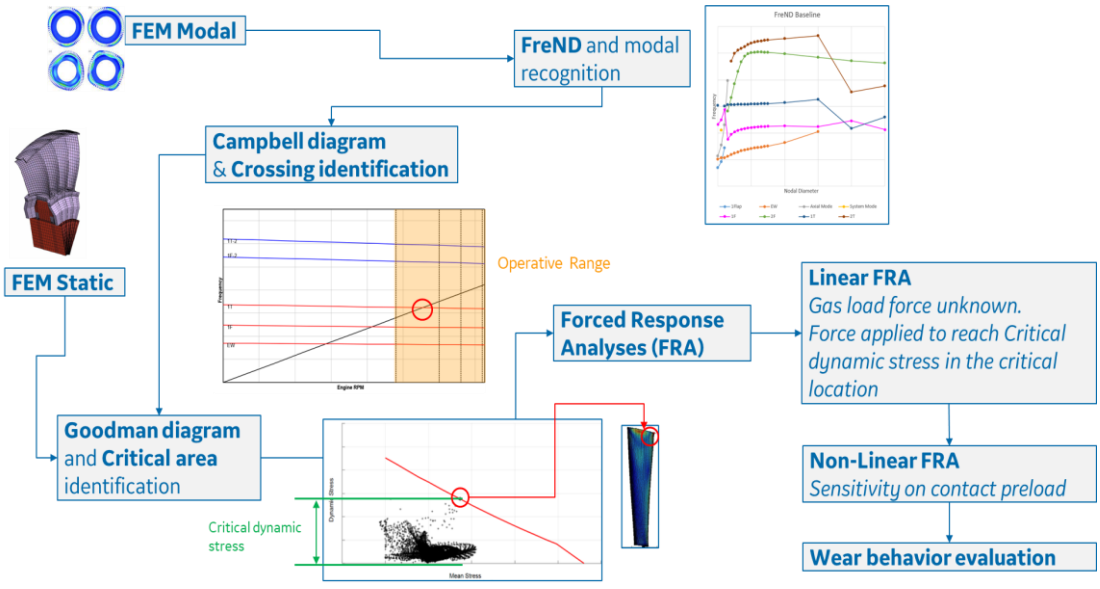

Figure 30: Workflow [36]

7.3 Forced Response Analyses (FRA)

7.3.1 Preprocessor

The software used for forced response analyses is called Policontact. The main steps in preprocessor section are the following:

- DB identification, necessary for the model identification process. In this step, it is possible to import the selected components which can be useful in the analyses
- CB-CMS Reduction, which is a reduced order modelling technique for a generic system with a friction contact interface
- Tran method, used for cyclic symmetry structures

Blade and disk are reduced as a single element component with 100 CB modes in cyclic symmetry condition. Master nodes are defined for contact pairs (at the interlocking interface), cyclic symmetry pairs and accessory master (which contains the maximum displacement node used for forced response analyses). The contact is at the interlocking surfaces with a local reference system.

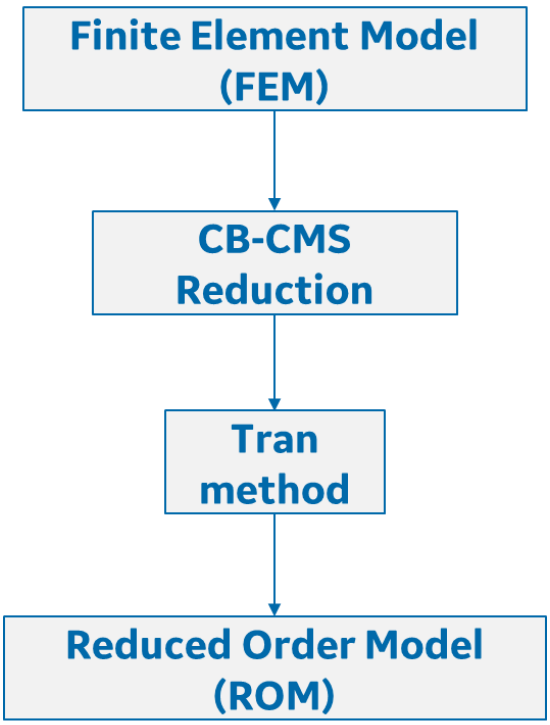

Figure 31: Steps for model reduction

The main advantage of the reduction is that the model degrees of freedom changes from 2 million to only 20k. This step is essential to study the forced response analyses within a reasonable time.

7.3.2 Linear and Non-Linear Forced Response Analyses

In linear FRA, there is no contact at the interlocking interface and there are only external forces due to aerodynamic load force.

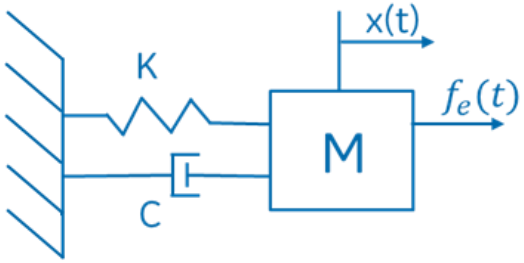

Figure 32: Reduced order model for linear FRA

With the linear FRA results, it is possible to compare the ROM frequencies with FEM frequency for checking the reduction goodness.

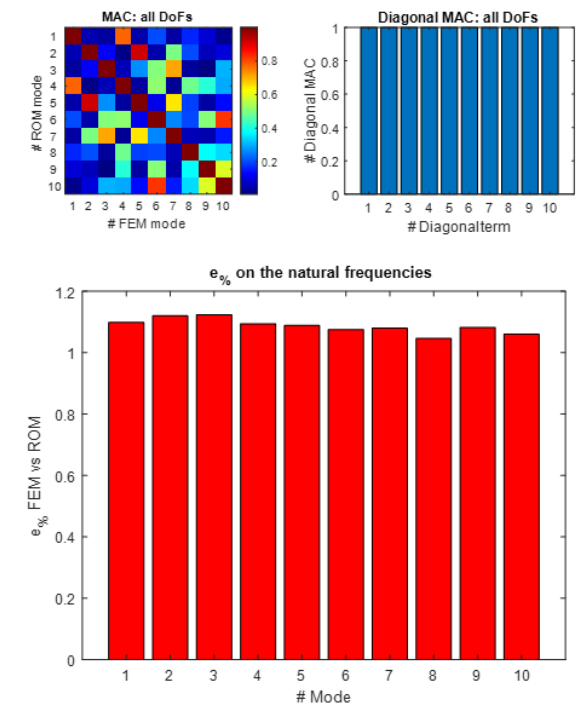

Figure 33: Reduction goodness

In non-linear FRA, it is necessary to consider the influence of non-linear contact at the interlocking interface. Rise of non-linear force f_{nl} on the contact surfaces to build the performance curve of the contact.

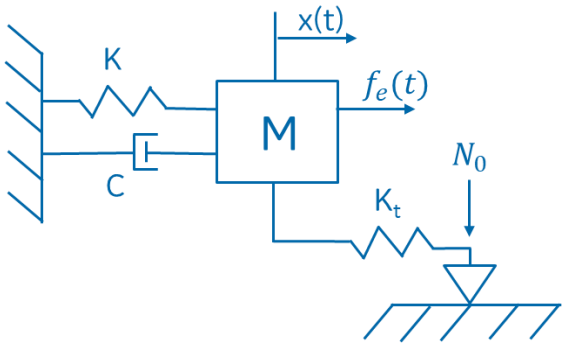

Figure 34: Reduced order model for non-linear FRA

7.3.3 FRA Results

Linear analyses are performed for tip free and full stick condition at interlocking interface. Tip free means that there is no contact surface at interlocking interface, so the blades are free to move, while full stick means that the contact does not slip.

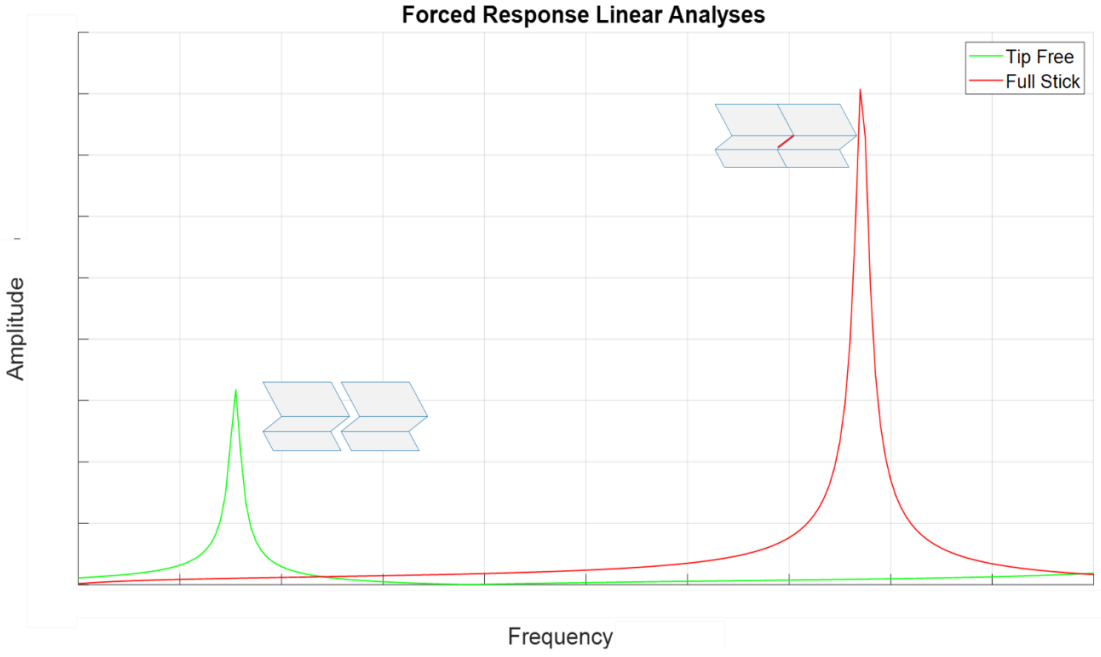

Figure 35: Linear FRA

Non-linear analyses are performed for several preload values, in order to build the performance curve. Preload at the interlocking interface depends on geometry, aerodynamic forces, contact interface and dynamic behavior of the blades. Amplitude vibration increases with higher preload, in according with the results obtained in the non-linear analyses.

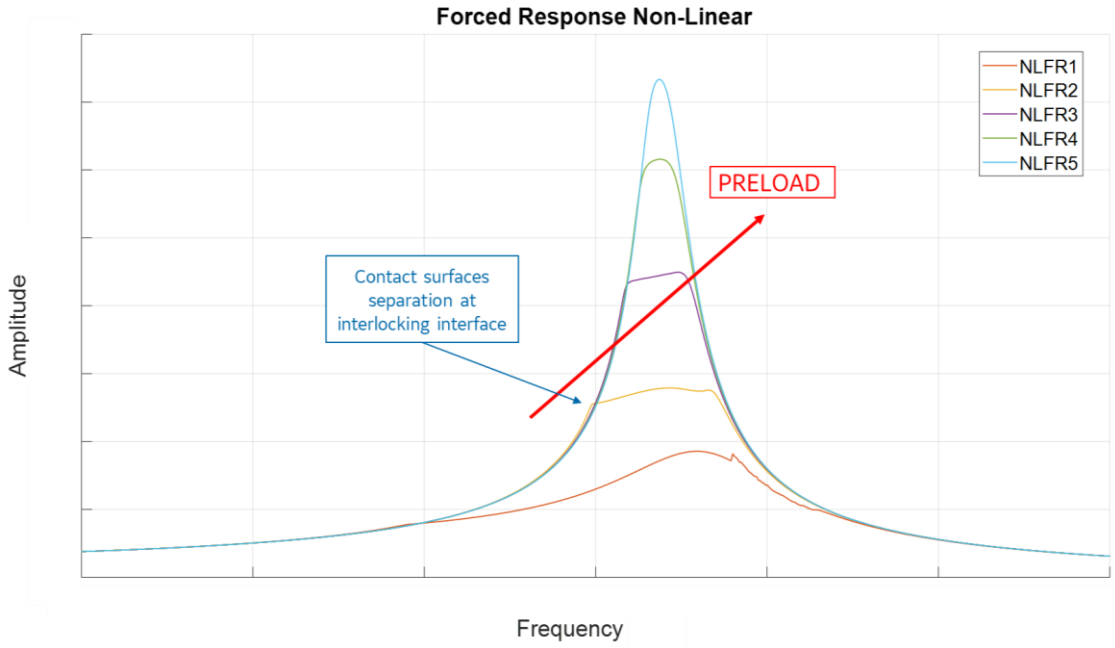

Figure 36: Non-linear FRA

Comparing linear and non-linear analyses in the same plot, it is possible to highlight that for the highest preload values, the peak of the non-linear analyses approaches to the peak of the linear analyses. This phenomenon is due to the very high preload values supposed in the linear analyses.

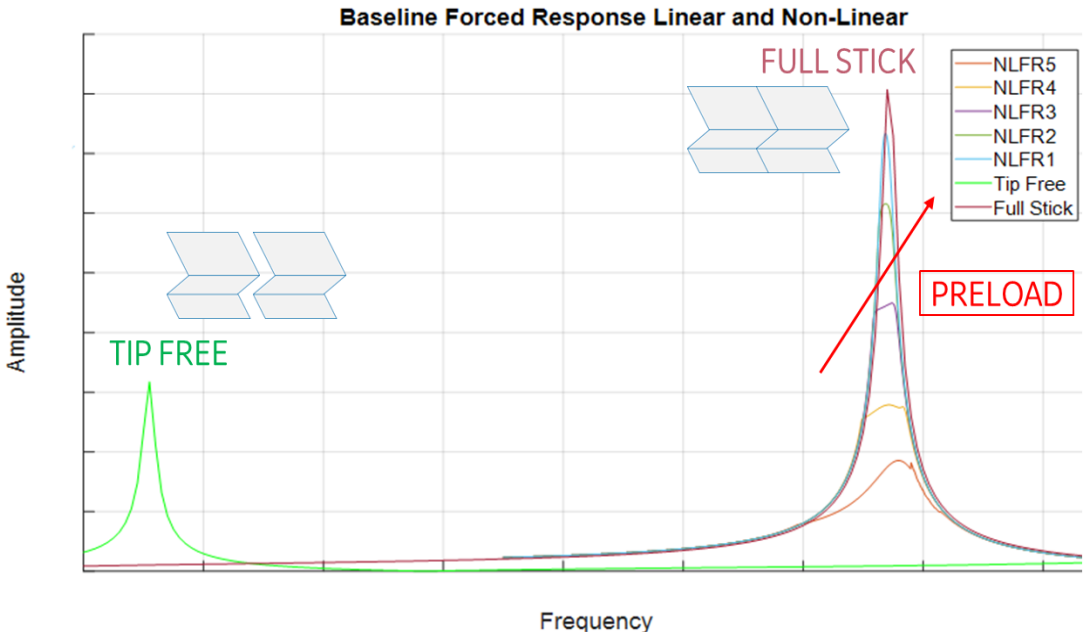

Figure 37:Linear and Non-Linear FRA

7.3.4 Change of the interlocking angle

The main goal of this thesis work is to study the impact on forced response analyses of variation of the interlocking angle, considering a new model with the same boundary conditions and loads of the previous one.

From this point on, we consider two blade models where the only difference is on the geometry of interlocking. The new model, called Redesign model, will have a new interlocking angle, so this change will impact on contact area and contact preload.

Increasing interlocking angle means that contact area and contact preload will increase too, so this will affect the dynamic behavior of the blade.

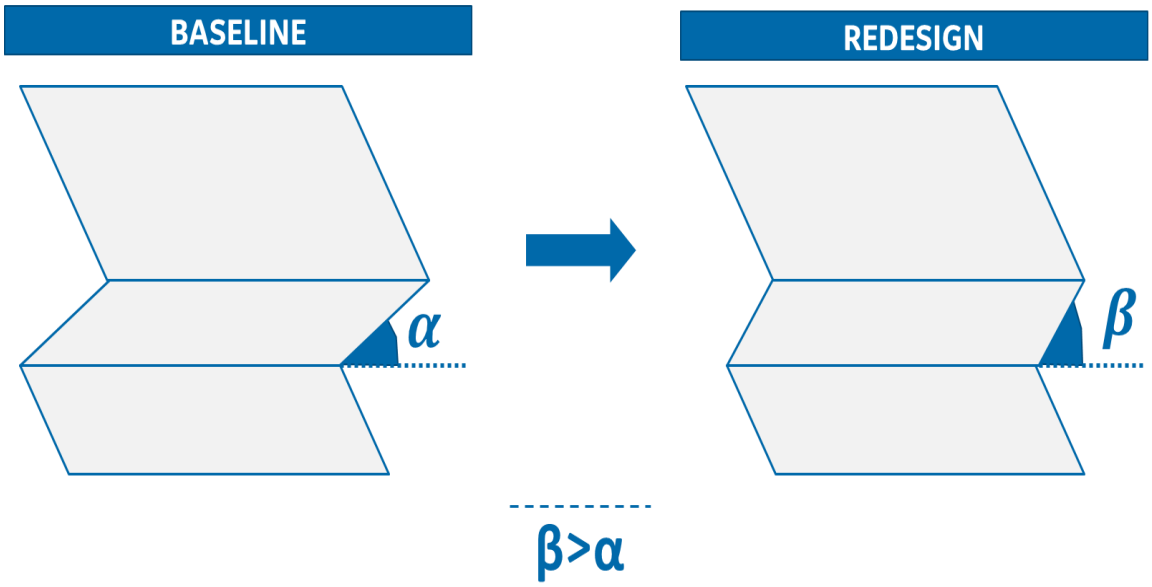

Figure 38: Change of interlocking angle from Baseline to Redesign model

In the Baseline model, it is necessary to find the critical dynamic stress in the critical location, called $\sigma_{baseline,a,crit}$, which is the stress value that makes the blade HCF critical, known from Goodman diagram.

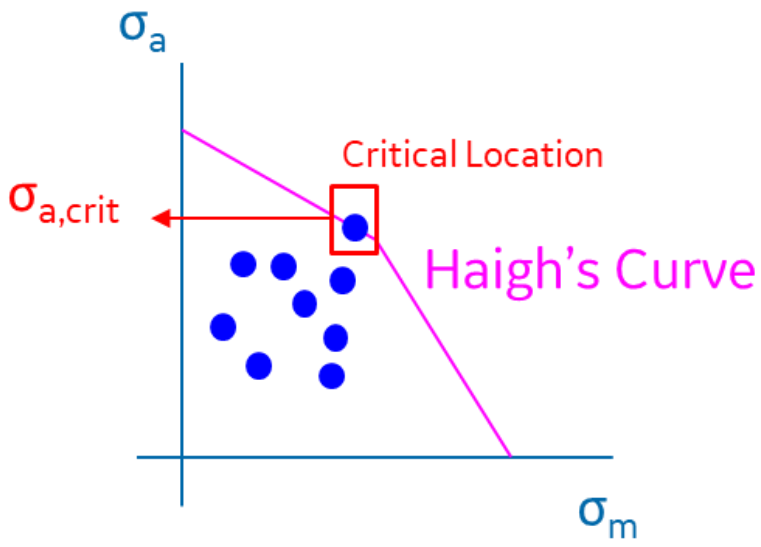

Figure 39: Modus operandi

It is necessary to find the critical load in forced response analyses, because the aerodynamic load is unknown. The followed strategy is to apply a unitary load in the node of maximum displacement and iteratively increasing or decreasing the force value since the dynamic stress in the critical location will be coincident to $\sigma_{baseline,a,crit}$.

Except the variation of interlocking angle, the Baseline and Redesign models are geometrically equivalent, so in Redesign model will be applied the same force of Baseline model in the node of maximum displacement. After FRA, it is necessary to compare the new stress value in the Redesign configuration with the dynamic stress of the Baseline model.

So, the comparison between Baseline and Redesign model is done on dynamic stress at the critical location using a frequency scale factor.

$$Frequency\ scale\ factor = \frac{z_{modal}}{z_{NL\_FRA}}$$

7.3.5 Comparison between Baseline and Redesign model

First comparison is done on linear FRA. Full stick peak is nearly coincident in both models, while tip free peak is not at the same frequency. Redesign model has tip free condition at a lower frequency, due to the different dynamic behavior of the blade.

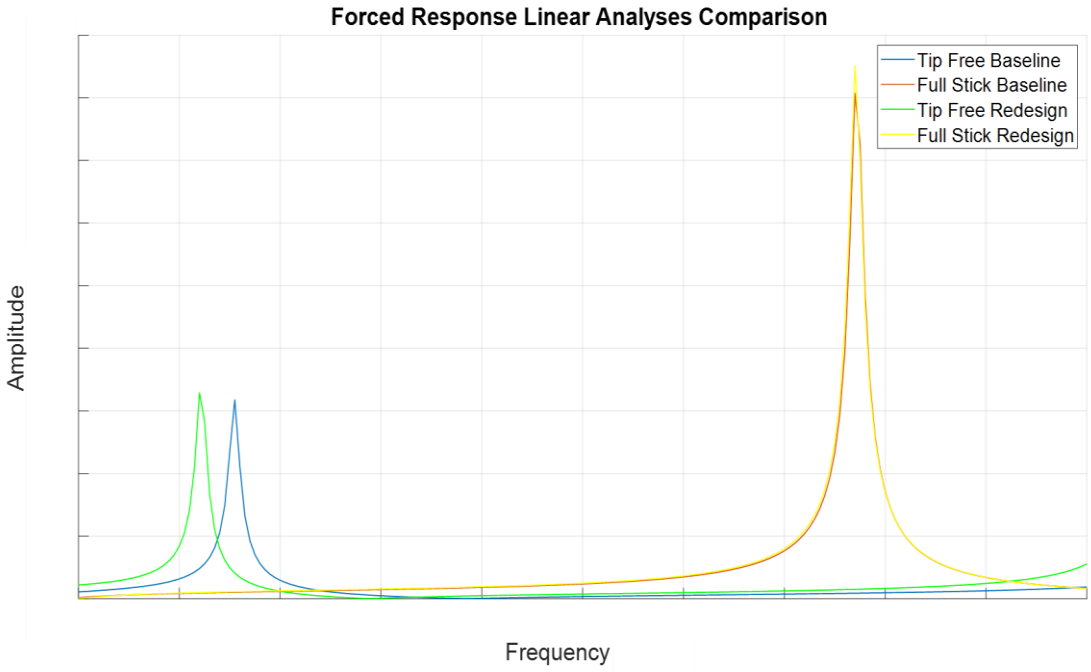

Figure 40: Linear FRA comparison

In non-linear FRA there are the main differences between the two configurations.

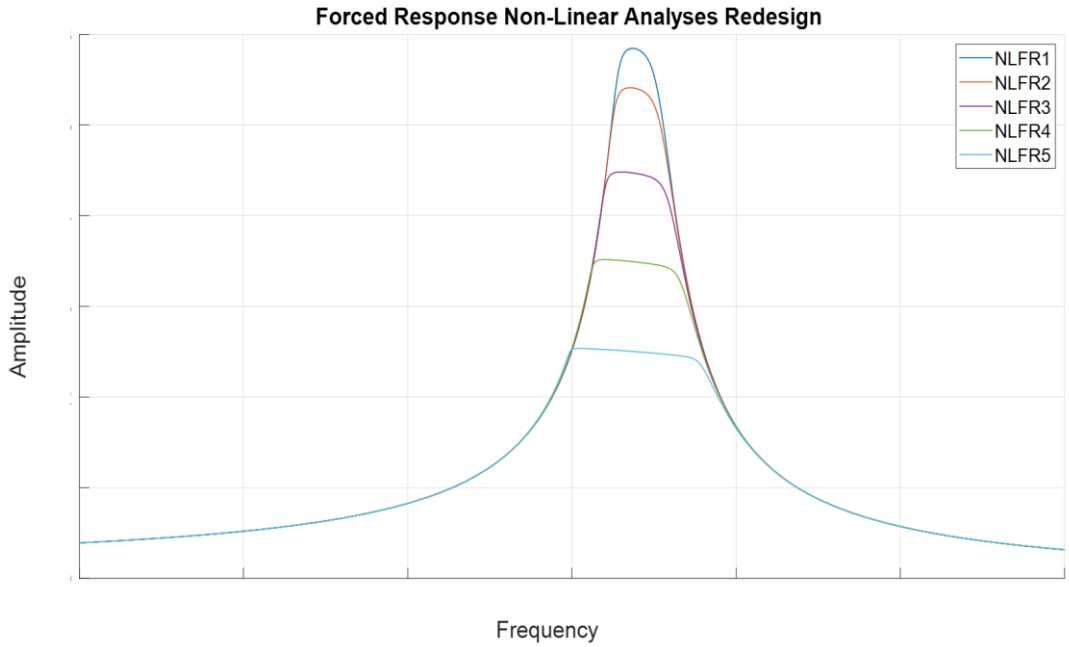

Figure 41: Non-linear FRA Redesign model

In non-linear FRA, the contact preload at interlocking interface in the Redesign model increased by 21% compared to the Baseline model. Instead, the amplitude of vibration is decreased by 26.8% in Redesign model, due to the different dynamic behavior between the two models.

Furthermore, the peaks of non-linear FRA in Redesign model are flatter than the Baseline model because the linear full stick peak is further away. So, the blades in Redesign model operate in a condition with higher contact preload but lower amplitude vibration.

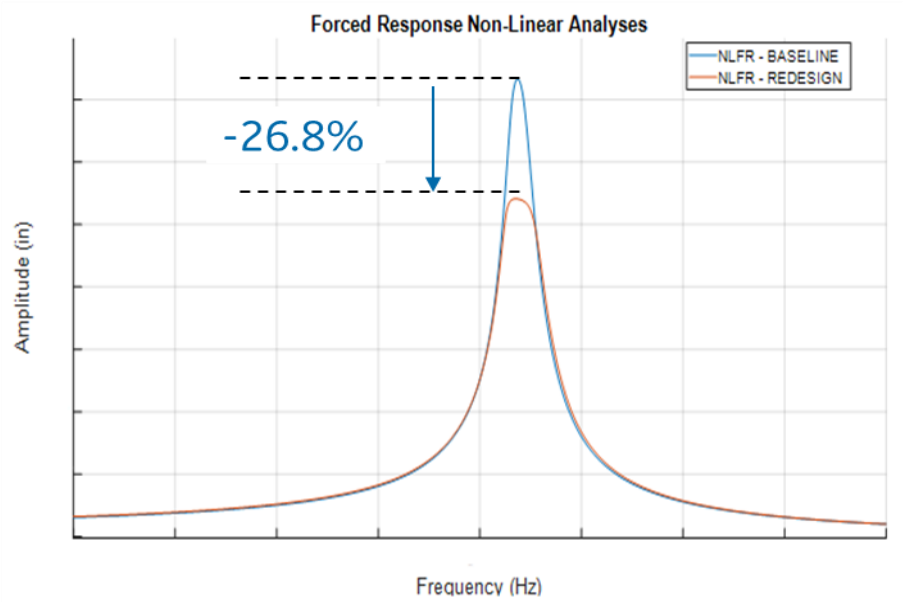

Figure 42: Non-linear FRA Comparison

Doing the sensitivity on contact preload, it is possible to build the so-called performance curve, where the amplitudes vibration are represented as a function of the contact preload.

Both models lay in stable branch of the performance curve. In the box below on the right, a typical performance curve is represented. The left branch is the unstable branch, where when preload decreases the amplitude vibration increases. This is a critical situation because the wear of the blades causes a decrease of preload, so if the amplitude of vibration increases, an HCF failure can occur. In the situation of Baseline and Redesign models, a preload decrease due to the wear causes a decrease of amplitude vibration.

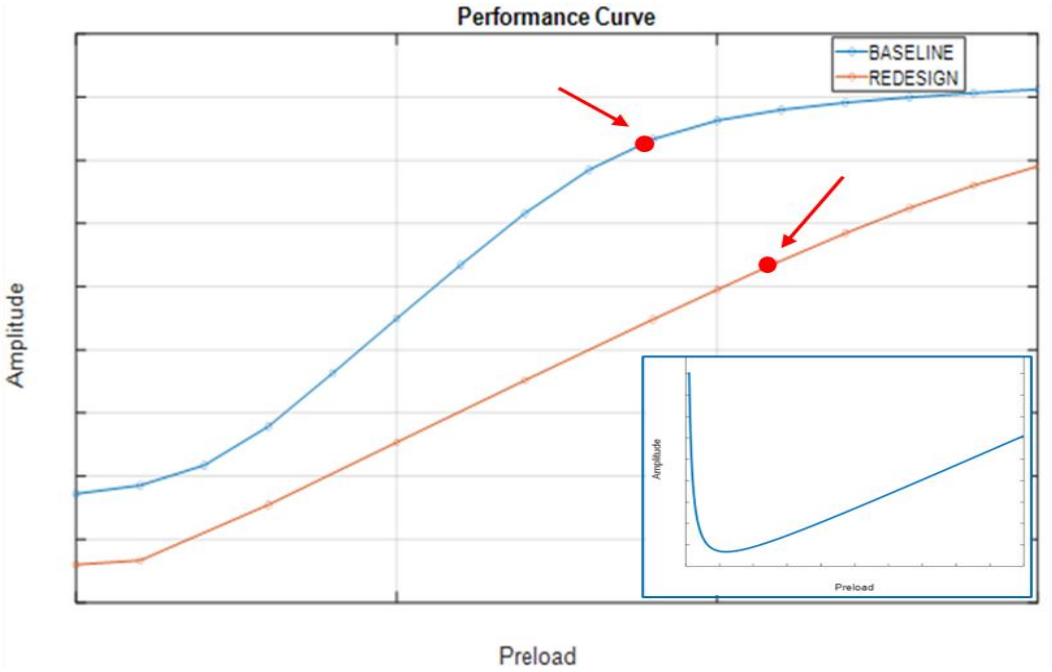

Figure 43: Performance Curve

The next step is to compare the dynamic stress in critical location obtained for the two configurations. In Redesign model the dynamic stress is reduced by 32%, so this means that increasing interlocking angle lead Redesign model to better HCF capability.

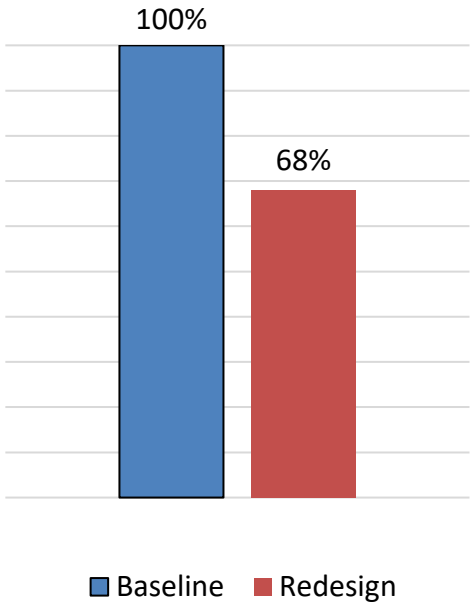

7.3.6 Hysteresis loop

Hysteresis is the dependence of the state of a system on its history. It is a phenomenon whereby the value assumed by a variable dependent on others is determined not only by the instantaneous values of the latter, but also by the values they had previously assumed.

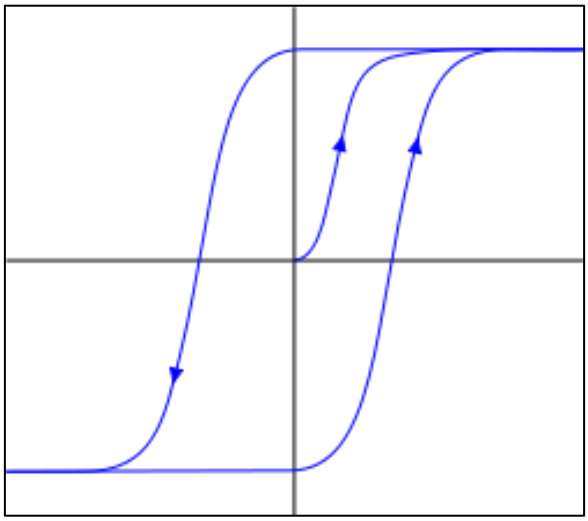

Figure 44: Ideal hysteresis loop [37]

The area of the hysteresis loop represents the dissipation of the blade on a single loop. The larger the area, the greater the dissipation will be.

In Baseline model, the area of hysteresis loop is very small, so there is a low contact dissipation. Along x-axis, the blade starts in stick condition and the loop follow the curve of lower Coulomb limit, so the contact is stuck. Then there is a slip condition, so the contact dissipates the energy until the loop curve ends again on the curve of upper Coulomb limit. Then the contact force goes to zero, so this is a lift-off condition. The hysteresis loop ends with a stick condition and then it restarts.

Instead, in Redesign model the area of hysteresis loop is larger than Baseline model, so the contact dissipation will be greater. Along x-axis, the blade switch from slip condition to stick condition during the cycle and the hysteresis loop shape approaches to the ideal hysteresis loop one.

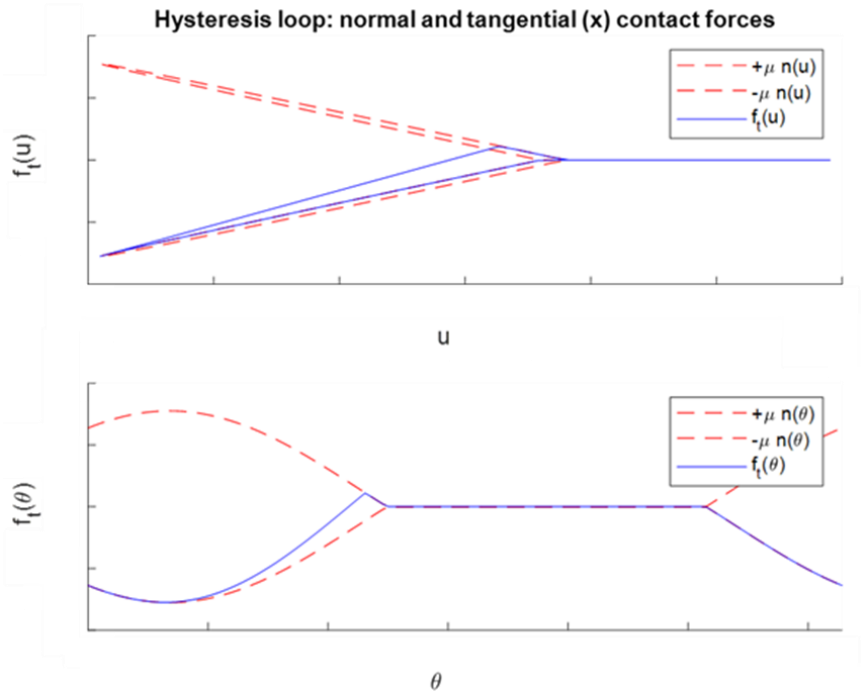

Figure 45: Baseline hysteresis loop along x-axis

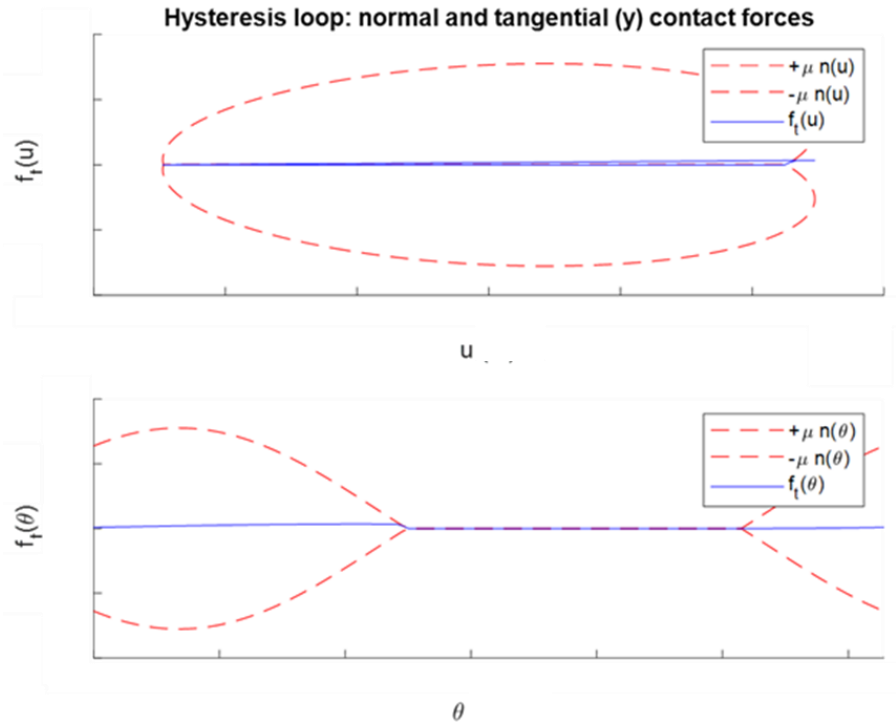

Figure 46:Baseline hysteresis loop along y-axis

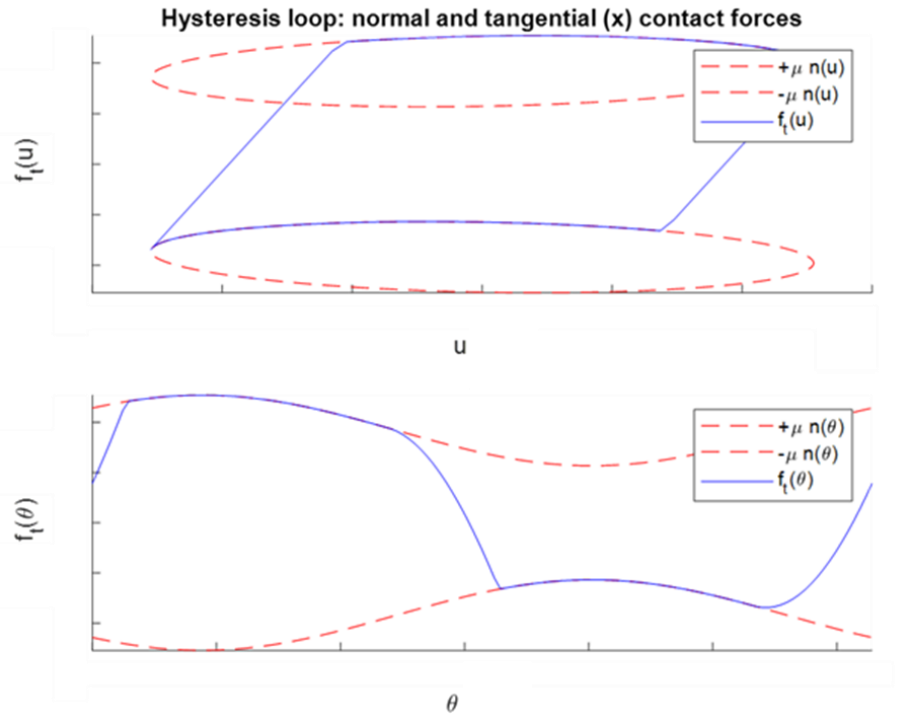

Figure 47:Redesign hysteresis loop along x-axis

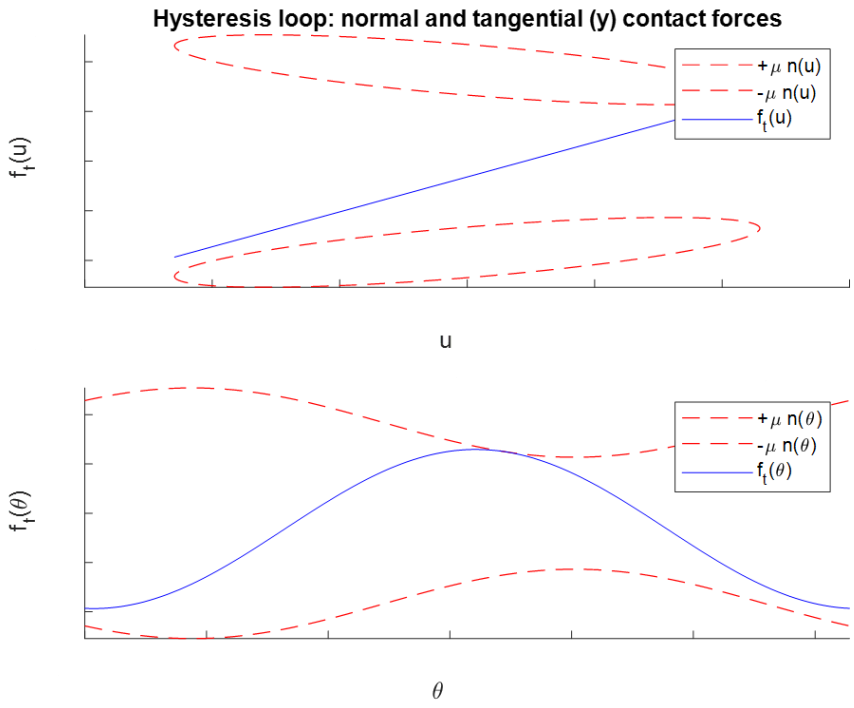

Figure 48:Redesign hysteresis loop along y-axis

7.4 Wear Analyses

In this section the focus is on the main differences on the wear behavior between Baseline and Redesign configuration.

Fretting wear is a dissipative phenomenon whose positive aspect is to reduce vibrations due to the interaction between gas flows passing through the blades. Due to the rubbing at the interlocking interface, the energy absorbed by the structure is dissipated as heat generation or removed volume, so it can wear out the components.

The software used for wear analyses is called Poliwear, that uses the Policontact FRA results to study the wear behavior of the blade.

The main steps of the procedure are the following:

- Contact model definition, which means the geometry definition of the two contact surfaces at the interlocking interface. In this case, cylinder-plane interface is selected since the contact area is not perfectly plain. The other options are plane-plane, cylinder-cylinder, sphere-plane, sphere-sphere, and they are all valid for the study of wear behavior. The hypothesis used for the contact geometry definition is the infinite half-space one, so the three-dimensional problem can be described through a set of normal equation and a set of tangential equation. Furthermore, it is assumed that the material has an isotropic linear elastic behavior.

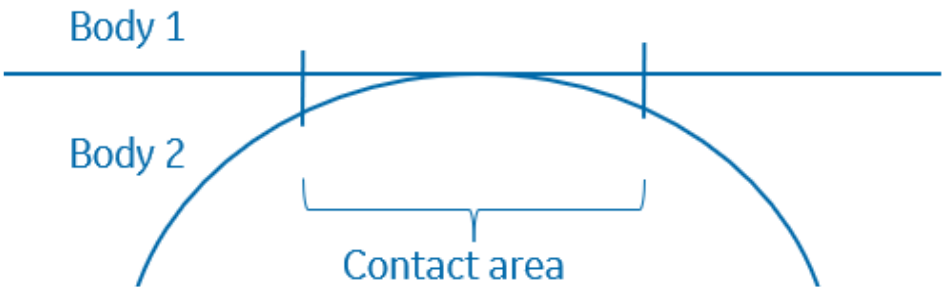

Figure 49: Contact model

- Contact plane discretization. The contact region over which the function will be integrated is a rectangular domain of dimensions N x N. Pressures

are evaluated in the center of the cells and considered uniform within the single cell.

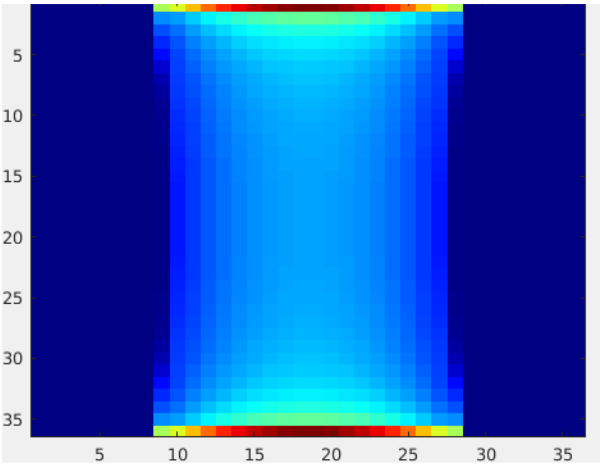

Figure 50:Discretization grid

- Contact normal solution and tangential solution. For the resolution of the contact problem, three of the most efficient methods are implemented and they are: Cholesky decomposition, conjugate gradient method and conjugate gradient method related to discrete Fourier transforms. The first is a direct method, the others are iterative methods.
- Wear law. The wear law used derived from Archard's law, and it is related to the energy dissipated by the contact during the hysteresis loops. It is applied after obtaining the normal and tangential contact solutions. The expression of the wear law is the following:

$$\Delta h = \frac{\alpha_{ref}}{4\delta_{0,ref}} \sum_{N\ cycles} \left(\sum_{1\ cycle} |\Delta s^t| \cdot \sum_{1\ cycle} q^t \cdot \Delta s^t \right)$$

Where:

- α_{ref} wear coefficient
- $\delta_{0,ref}$ sliding width for zero tangential load
- $q^t \cdot \Delta s^t$ is the energy dissipated during a time increment (q is the stress, Δs is the approach variation) expressed in J/mm^2
- Δh removed height expressed in mm

The main difficult is to estimate the wear coefficient which links the energy dissipated to the removed material. All the coefficient used in the analyses are obtained by experimental test.

- Removed volume results.

The main input parameters necessary for the wear analyses are the following:

- Material: elastic modulus E and Poisson coefficient ν
- Loads: normal load at the contact plane. By the previously analyses, the value of preload for Redesign model is increased by 21% as compared to the preload of Baseline model
- A-dimensional coefficients: friction coefficient μ, wear rate α and wear coefficient γ. All these coefficients are given by experimental test

Then it is necessary to define the input cycle parameters:

- Number of iterations
- Number of profile update iterations: to speed up the calculation. Each time Poliwear executes an iteration, it updates the worn surfaces proportionally to this parameter
- Number of output update iterations: it specifies the refresh rate of graphical and textual outputs

For Baseline and Redesign model, the number of iterations overall is about 110 billion of cycles.

The first wear analyses are done for a low number of cycles, because it is necessary to verify that the pressure results match the analytical results provided by Hertzian theory. The main equations of the Hertzian theory used are the following:

- Contact area radius

$$a = \left(\frac{3PR}{4E^*}\right)^{\frac{1}{3}}$$

- Max pressure

$$p_0 = \frac{3P}{2\pi a^2}$$

- Pressure distribution

$$p = p_0\left[1 - \left(\frac{\mathrm{r}}{\mathrm{a}}\right)^2\right]^{\frac{1}{2}}$$

The pressure comparison shows that in both models, the numerical results match the analytical results provided by the Hertzian theory. The differences between the two curves are due to the discretization of the contact area. In the figures, the distribution of pressures in correspondence of the median line of the contact area is represented.

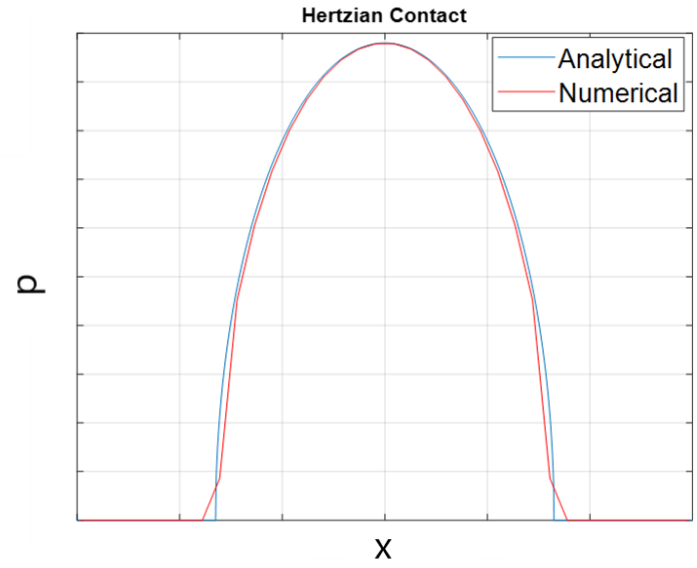

Figure 51: Pressure comparison Baseline model

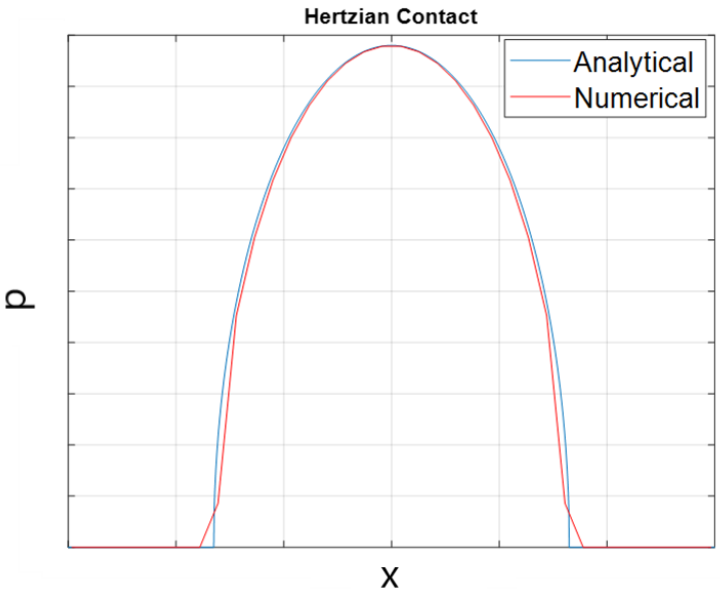

Figure 52: Pressure comparison Redesign model

7.5 Wear Results

From the results of wear analyses, Redesign model has a higher wear consumption (+17% of removed volume) than Baseline model after about 110 billion of cycles.

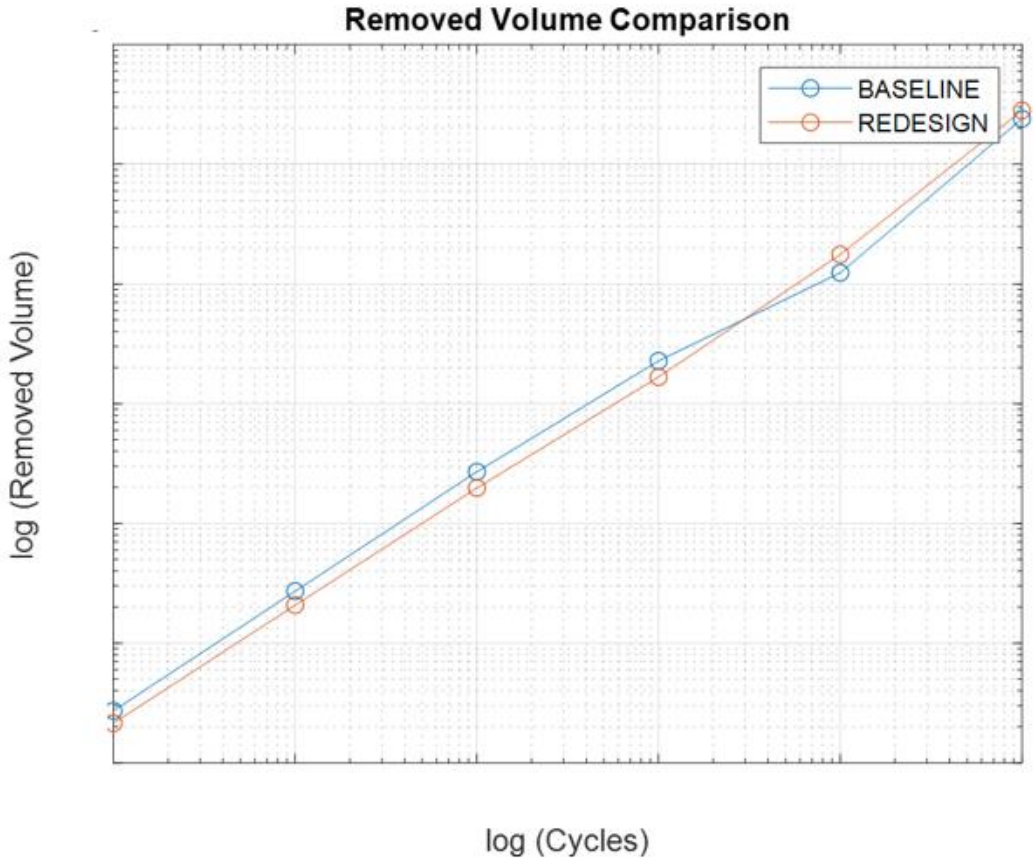

Figure 53: Removed volume comparison

Due to the high contact preload values, in both configurations the wear doesn't start from the center of the cylinder because it is in stick condition. The center of the contact area is stuck so it doesn't slip, and it doesn't dissipate the energy.

Now, the evolution of removed volume after each cycle iterations is represented for both configurations:

- 1'000'000 cycles

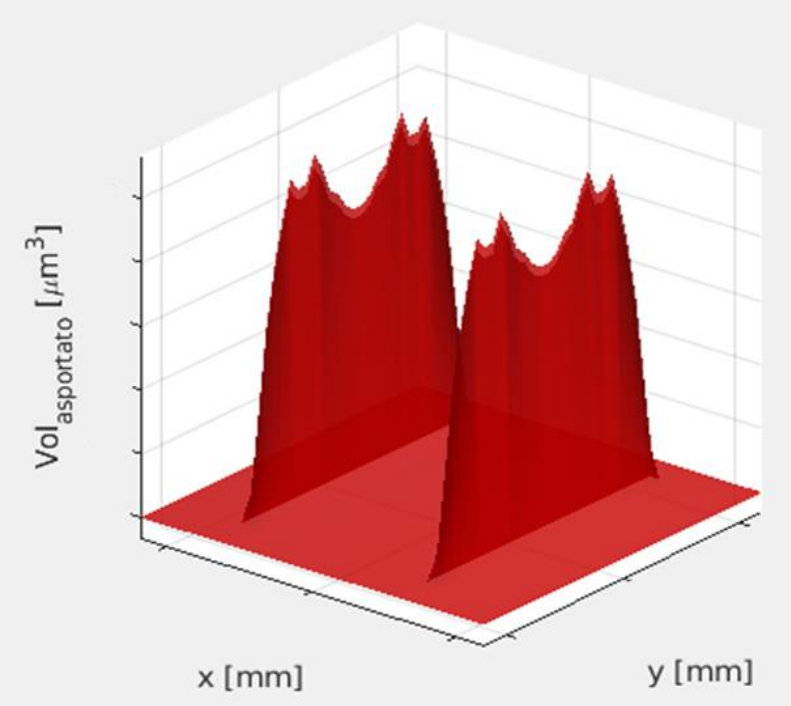

Figure 54: Removed volume for Baseline model after 1'000'000 iterations

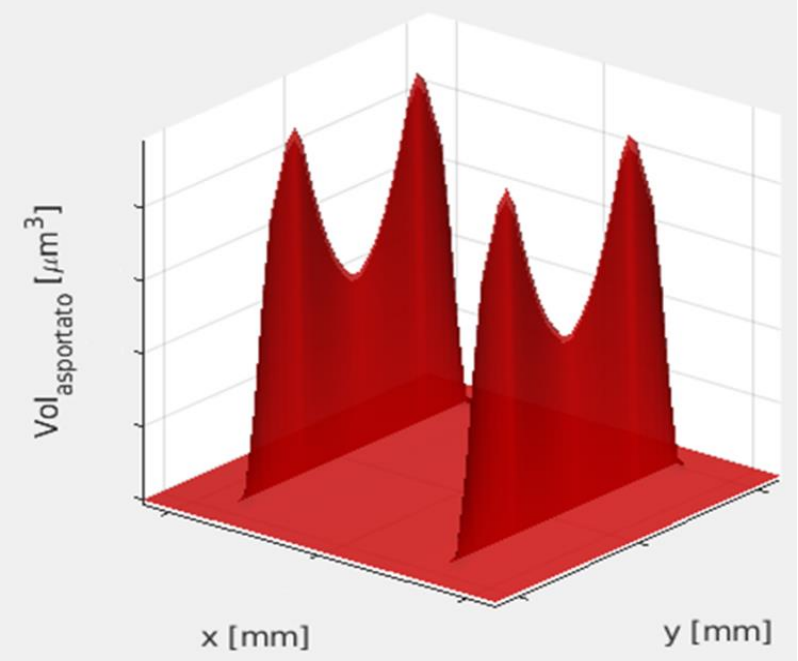

Figure 55: Removed volume for Redesign model after 1'000'000 iterations

- 10’000’000 cycles

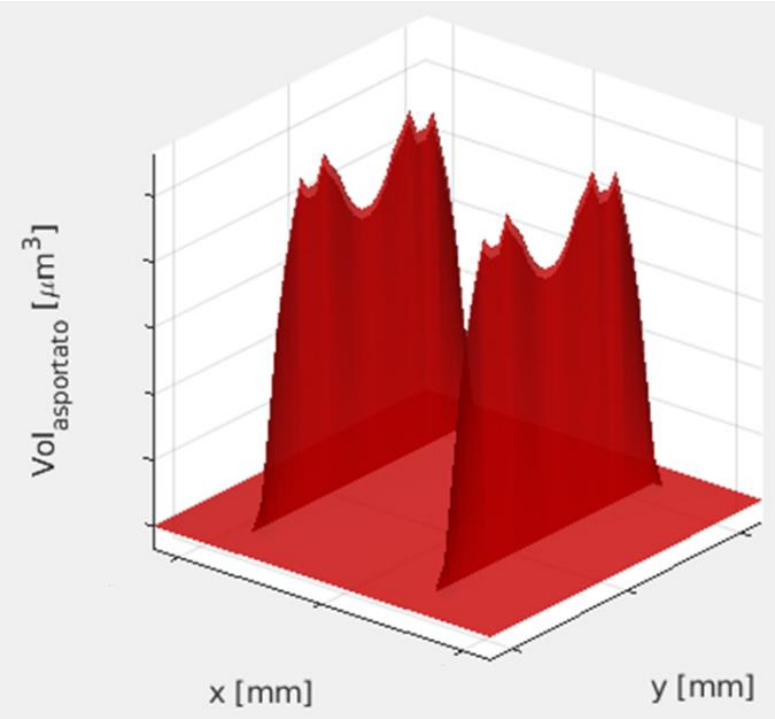

Figure 56: Removed volume for Baseline model after 10'000'000 iterations

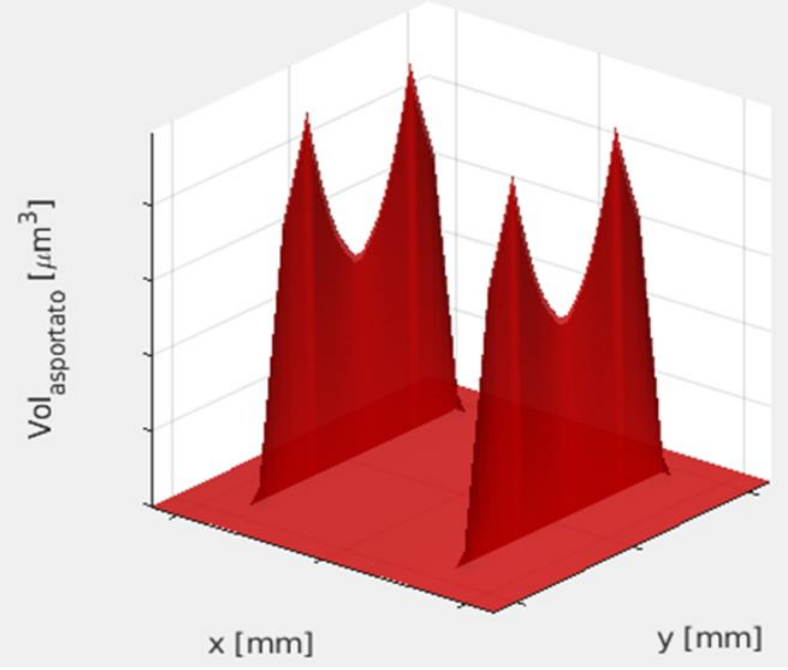

Figure 57: Removed volume for Redesign model after 10'000'000 iterations

- 100’000’000 cycles

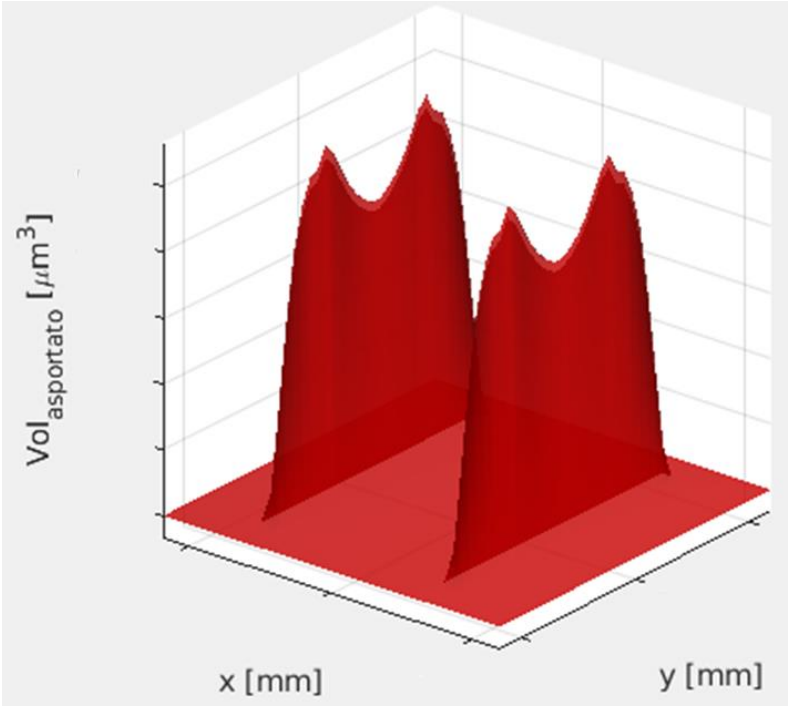

Figure 58: Removed volume for Baseline model after 100'000'000 iterations

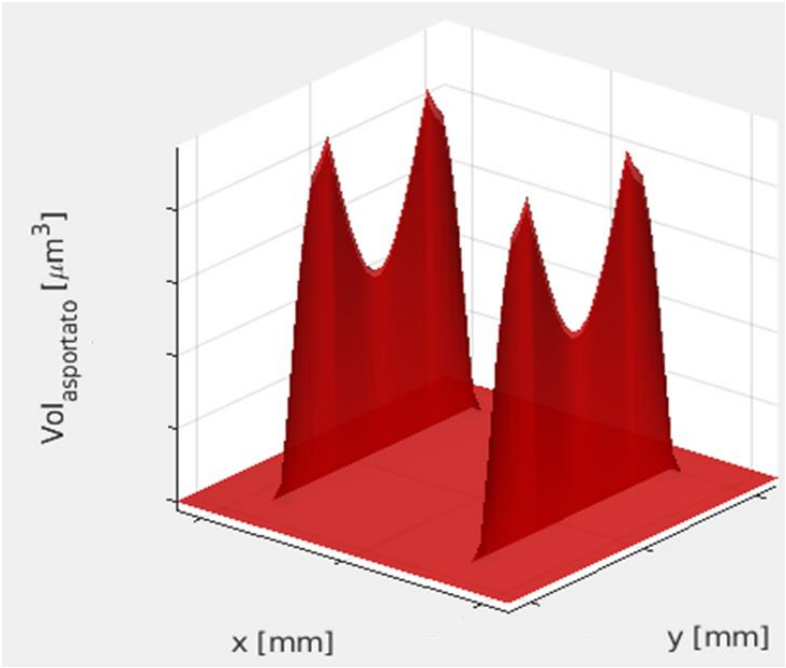

Figure 59: Removed volume for Redesign model after 100'000'000 iterations

- 1’000’000’000 cycles

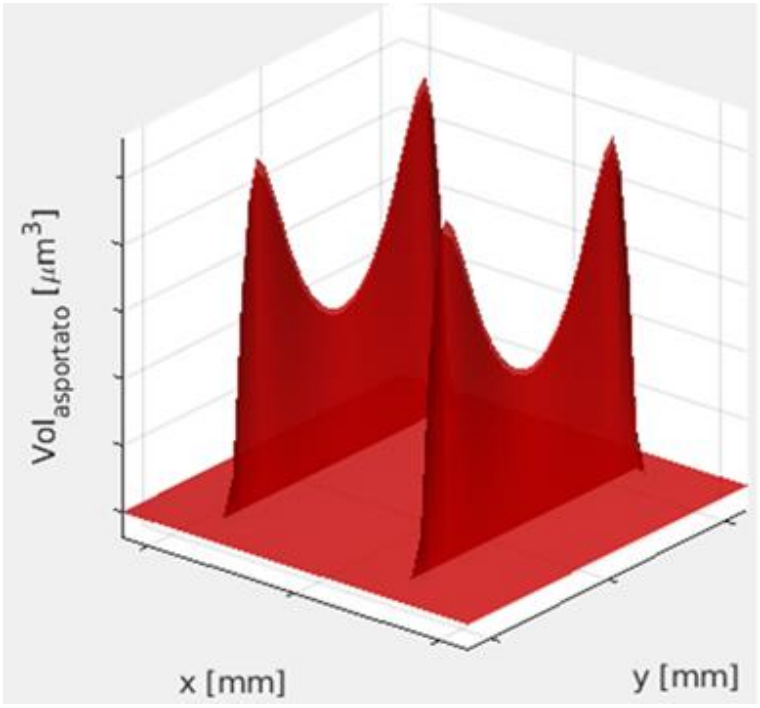

Figure 60: Removed volume for Baseline model after 1'000'000'000 iterations

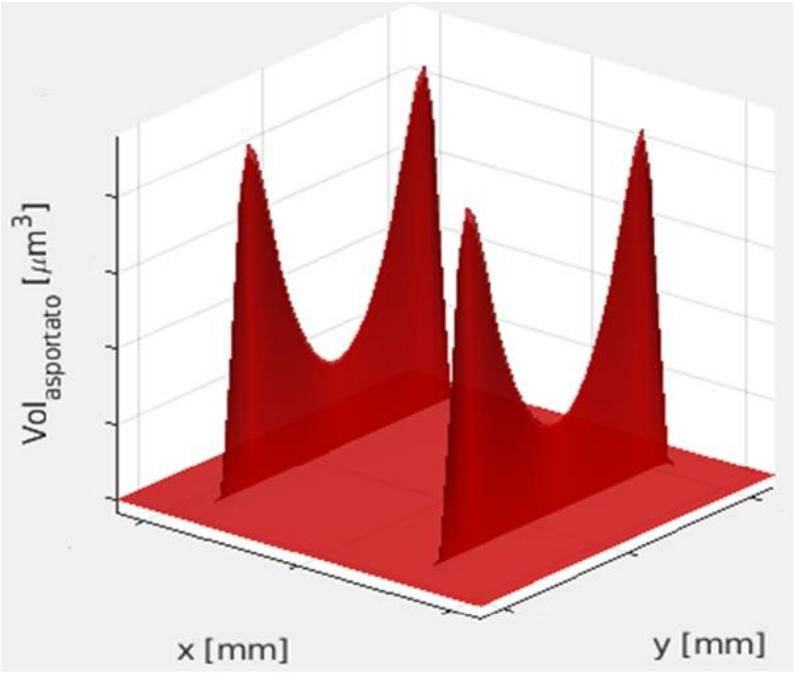

Figure 61: Removed volume for Redesign model after 1'000'000'000 iterations

- 10’000’000’000 cycles

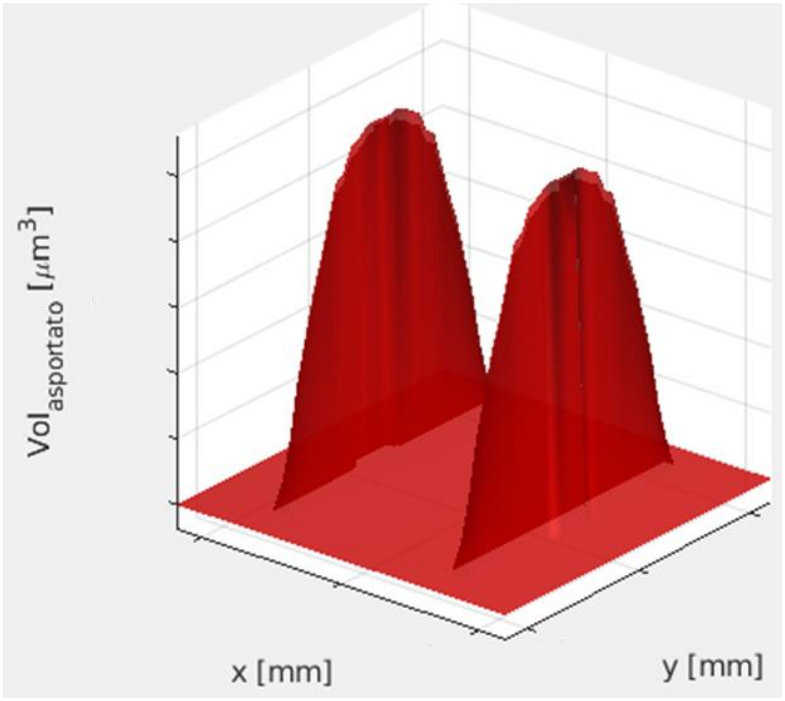

Figure 62: Removed volume for Baseline model after 10'000'000'000 iterations

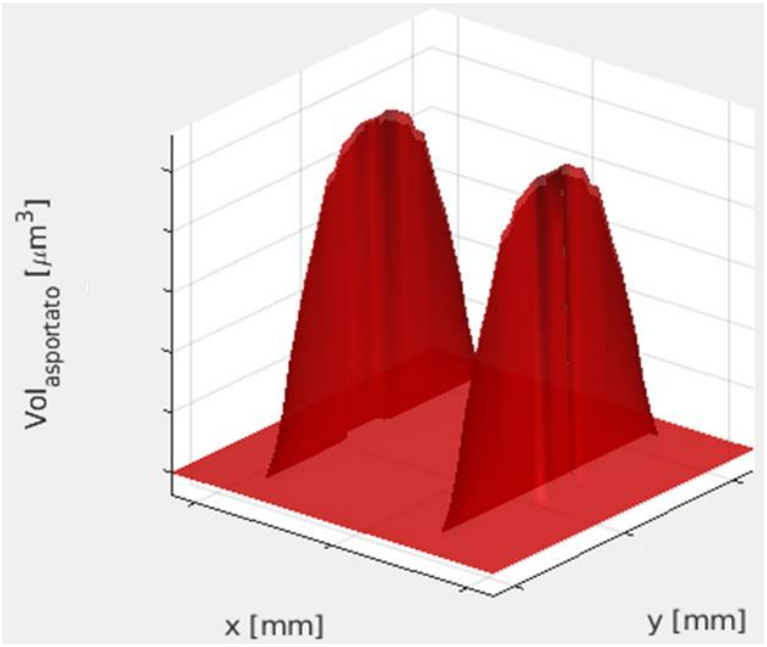

Figure 63: Removed volume for Redesign model after 10'000'000'000 iterations

- 100’000’000’000 cycles

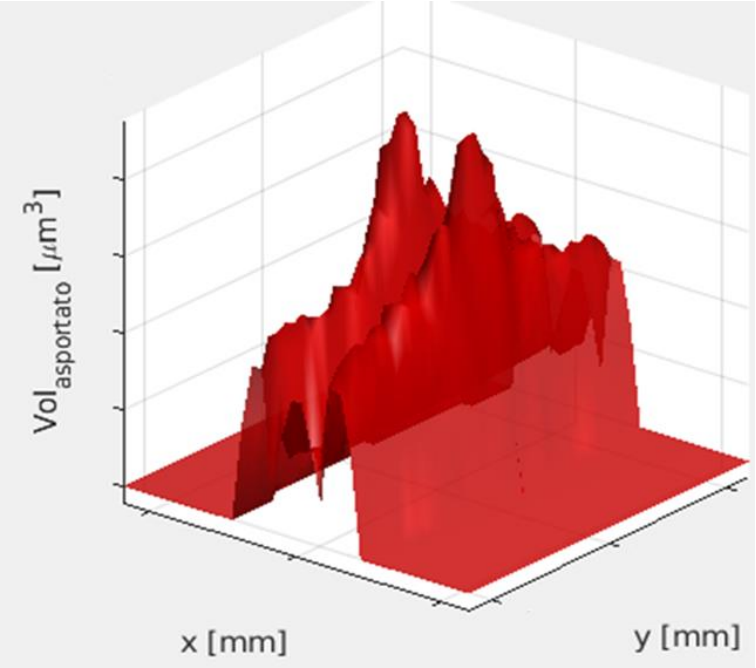

Figure 64: Removed volume for Baseline model after 100'000'000'000 iterations

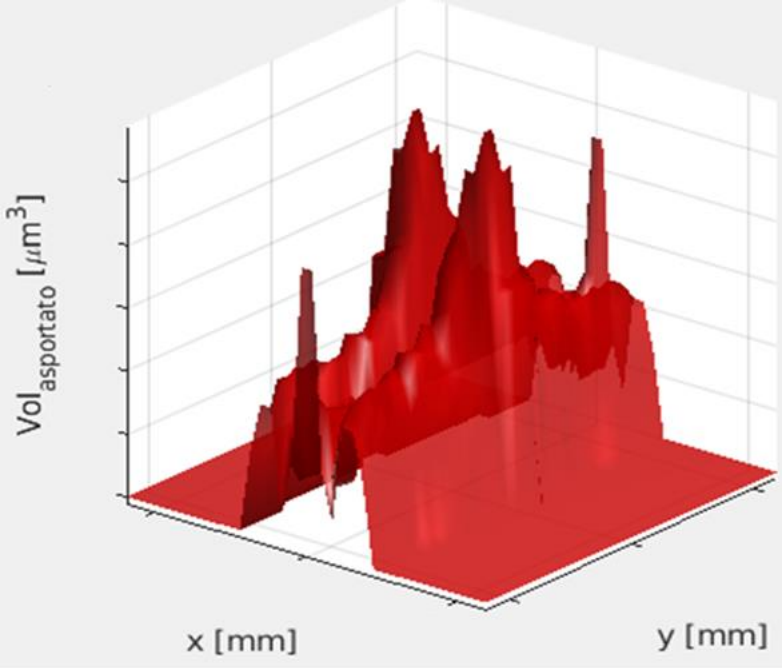

Figure 65: Removed volume for Redesign model after 100'000'000'000 iterations

Another important result is given by the time evolution of the profile of body number 1 along the horizontal and vertical axis of the grid (2D) and the separation between the two contact surfaces at the initial and final instant of the simulation (3D).

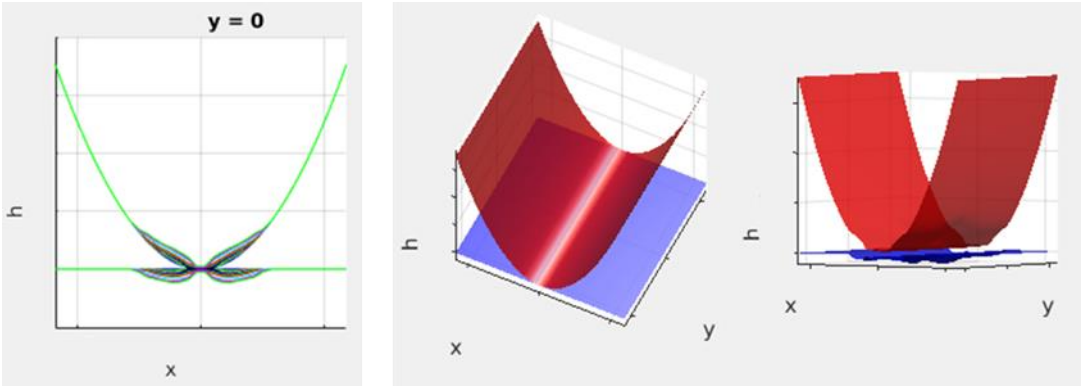

Figure 66: 2D and 3D profile for Baseline model

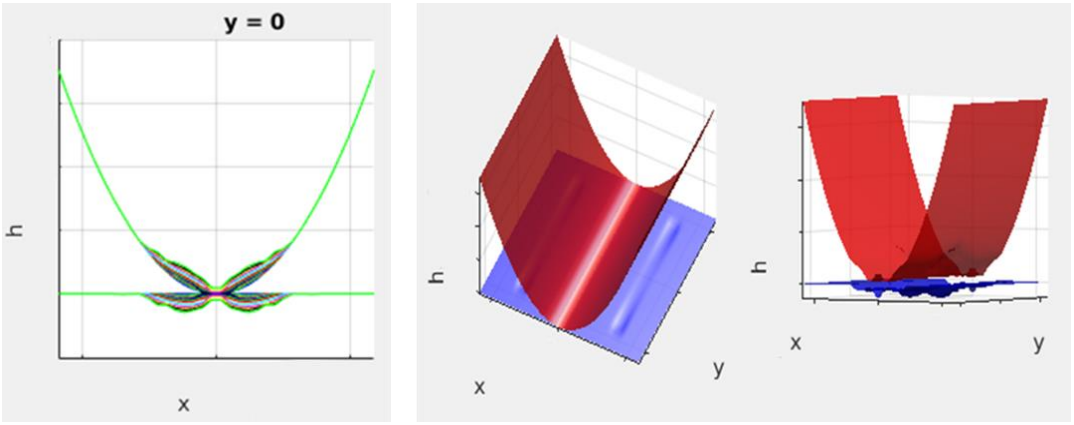

Figure 67: 2D and 3D profile for Redesign model

The last result is the contact area remained after 110 billion cycles. Due to the higher contact preload, the center of cylinder is in stick condition, so it does not dissipate energy. For these reasons, the final contact area is only a thick layer at the center of cylinder for both configurations.

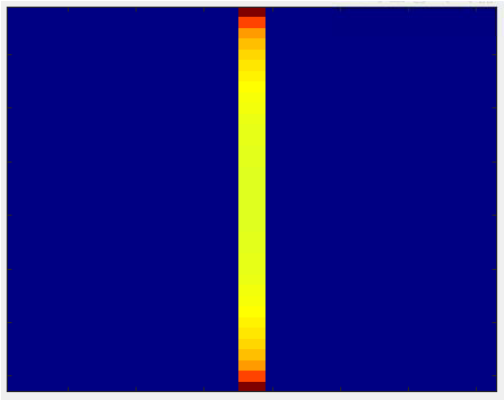

Figure 68: Contact area for Baseline model

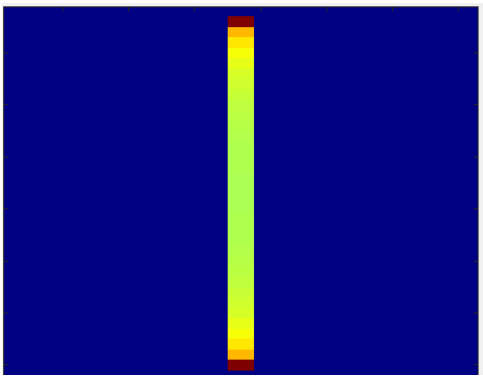

Figure 69: Contact area for Redesign model

Chapter 8

Conclusion

From the obtained results it is possible to infer the following considerations with regard of the forced response and wear behavior, respectively.

From forced response analyses, it has been obtained that:

- For Redesign model the amplitude vibration is lower than for Baseline model
- For Baseline model the contact dissipation is lower, due to the smaller area of the hysteresis loop
- For Redesign model the dynamic stress in the critical location is lower than for Baseline model

From wear analyses, we obtained that:

- Redesign model has a higher wear consumption than Baseline model
- Due to the high contact preload values, in both configurations the wear doesn't start from the center of the cylinder because it is in stick condition

The main consequences of these results are that increasing interlocking angle leads Redesign model to:

- Better HCF capability
- Higher wear volume consumed

From these results, it is not possible to say if one configuration is better than the other. It is necessary to properly evaluate forced response analyses and wear capability considering the effective blade dynamics loads, and the effective time for the shop visit (maintenance and replacement of the blades).

Bibliography

[1] Hill P.G., Peterson C.R., *Mechanics and Thermodynamics of Propulsion*, Addison-Wesley Publishing Company, 1992

[2] Rolls Royce, *The Jet Engine*, John Wiley & Sons, 2015

[3] Giuseppe Battiato, *Vibrations prediction and measurements of multi-stage bladed disks with non-linear behavior due to friction contacts,* PhD Thesis, Politecnico di Torino, 2017

[4] Lakshminarayana Reddy Tamatam, *Effect of wear on the dynamics of structures with friction contacts*, PhD Thesis, Politecnico di Torino, 2021

[5] G. Alvin Pierce and Dewey H. Hodges, *Introduction to structural dynamics and aeroelasticity,* Cambridge University Press, 2011

[6] Giancarlo Genta, *Dynamics of rotating systems*, Springer New York, 2005

[7] S. Mehrdad Pourkiaee and Stefano Zucca, *A reduced order model for nonlinear dynamics of mistuned bladed disks with shroud friction contacts*, Journal of Engineering for Gas Turbines and Power, 2019

[8] Randall J. Allemang, *The Modal Assurance Criterion – Twenty Years of Use and Abuse*, University of Cincinnati, 2003

[9] Miroslav Pastor, Michael Binda and Tomáš Harþarik, *Modal Assurance Criterion*, Procedia Engineering 48, pp. 543-548, 2012

[10] Valeria Pinto, *Aeromechanical Optimization of Aeronautical Low-Pressure Turbine Components*, Master Thesis, Politecnico di Torino, 2020

[11] Christian Fantino, *Caratterizzazione Dinamica di un Rotore LPT in presenza di Mistuning Intenzionale*, Master Thesis, Politecnico di Torino, 2018

[12] Valerio Piscopo, *Analysis of Multistage Structures using Cyclic Symmetry*, Master Thesis, Politecnico di Torino, 2022

[13] Marco Lassalle, *Self-excited vibrations controlled by damping at blade root joints of turbine disks*, PhD Thesis, Politecnico di Torino, 2018

[14] *Collar's Triangle,* URL: https://aerospaceengineeringblog.com

[15] Stefano Zucca, *Dispense del corso di Dinamica dei rotori per applicazioni aerospaziali,* Politecnico di Torino, 2019

[16] *Turbojet,* URL: https://en.wikipedia.org/wiki/Turbojet

[17] *Turboshaft,* URL: https://en.wikipedia.org/wiki/Turboshaft

[18] *Turbofan,* URL: https://en.wikipedia.org/wiki/Turbofan

[19] *Turboprop,* URL: https://en.wikipedia.org/wiki/Turboprop

[20] *Brayton cycle,* URL: https://en.wikipedia.org/wiki/Brayton_cycle

[21] *GE90,* URL: https://en.wikipedia.org/wiki/General_Electric_GE90

[22] *GE T64,* URL: https://en.wikipedia.org/wiki/General_Electric_T64

[23] Giuseppe Battiato and Christian M. Firrone, *A modal based reduction technique for wide loose interfaces and application to a turbine stator*, Mechanical Systems and Signal Processing Vol.139, 2019

[24] Giuseppe Battiato, Christian M. Firrone, Teresa M. Berruti and Bogdan I. Epureanu, *Reduction and coupling of substructures via Gram-Schmidt Interface modes*, Computer Methos in Applied Mechanics and Engineering Vol. 336 pp. 187-212, 2018

[25] Giuseppe Battiato and Christian M. Firrone, *A reliable Pre-Processing for the Simulation of Friction Joints in Turbomachineries and its Validation: A Case Study with Policontact*, GT2019-91764, 2019

[26] Robert J. Guyan, *Reduction of Stifness and Mass Matrices*, AIAA Journal pp. 3:380, 1965

[27] Su-Huan Chen and H. H. Pan, *Guyan Reduction*, Communications in Applied Numerical Methods Vol.4 pp. 549-556, 1988

[28] Roy R. Craig Jr. and Mervyn C. C. Bampton, *Coupling of Substructures for Dynamic Analyses*, AIAA Journal Vol. 6 No. 7, 1968

[29] Eleonora Caponio, *Calcolo della risposta forzata di componenti per motori aeronautici in presenza di contatti per attrito*, Master Thesis, Politecnico di Torino, 2018

[30] Jacopo Gregori, *Different loading configuration impact on non linear dynamic of airfoil in Low Pressure Turbine*, Master Thesis, Politecnico di Torino, 2021

[31] Miriam Zazza, *Validazione del software Policontact per il calcolo della risposta forzata di componenti aeronautici in presenza di contatti per attrito*, Master Thesis, Politecnico di Torino, 2019

[32] S. Mehrdad Pourkiaee, Stefano Zucca and Robert G. Parker, *Relative cyclic component mode synthesis: A reduced order modeling approach for mistuned bladed disks with friction interfaces*, Mechanical Systems and Signal Processing, 2021

[33] D. M. Tran, *Component mode synthesis methods using interface modes. Application to structures with cyclic symmetry*, Computer & Structure Vol. 79 pp. 209-222, 2001

[34] Rizwan Ahmed, Christian M. Firrone and Stefano Zucca, *Design and Calibration of a Tri-Directional Contact Force Measurement System*

[35] https://www.ihi.co.jp/msc/Application_Samples/Application_Samples.htm

[36] https://it.wikipedia.org/wiki/Isteresi

[37] L. Moroz, Y. Govoruschenko, L. Romanenko and P. Pagur, *Methods and Tools for Multidisciplinary Optimization of Axial Turbine Stages with Relatively Long Blades*, ASME Turbo Expo 2004, GT2004-53379